Enhancing the economic efficiency of cross-regional renewable energy trading via optimizing pumped hydro storage capacity

Xingjin Zhang[a,b], Edoardo Patelli[c], Ye Zhou[d], Diyi Chen[a,b], Jijian Lian[e], Beibei Xu*[a,b]

[a] *Institute of Water Resources and Hydropower Research, Northwest A&F University, Shaanxi Yangling 712100, China*
[b] *Key Laboratory of Agricultural Soil and Water Engineering in Arid and Semiarid Areas, Ministry of Education, Northwest A & F University, Shaanxi Yangling 712100, China*
[c] *Department of Civil and Environmental Engineering, University of Strathclyde, Glasgow, United Kingdom*
[d] *Institute of Hydraulic Machinery, Department of Operation Support, China Institute of Water Resources and Hydropower Research, Beijing, China*
[e] *Key Laboratory of Hydraulic Engineering Simulation and Safety, Tianjin University, Tianjin 300072, China*

***Corresponding author:** Beibei Xu
Mailing Address: Institute of Water Resources and Hydropower Research, Northwest A&F University, Shaanxi Yangling 712100, China
Telephones: 086-187-0080-9631
E-mail: xubeibei0413@163.com

Funding

This research is supported by National Natural Science Foundation of China (Grant No. K3010121624), Chinese Universities Scientific Fund (Grant No. 2452020210/Z1090220172), Basic and applied basic research fund of Guangdong Province (Grant No. 2021A1515110552), Scientific research fund of Inner Mongolia water resources and Hydropower Survey and Design Institute (Grant No. K4040121228).

CRediT authorship contribution statement

Xingjin Zhang: Conceptualization, Methodology, Software, Formal analysis, Investigation, Data curation, Writing – original draft, Visualization.
Edoardo Patelli: Writing – original draft, Supervision, Writing – review & editing.
Ye Zhou: Methodology, Writing – review & editing, Supervision.
Diyi Chen: Writing-Review & Editing, Funding acquisition, Project administration.
Jijian Lian: Writing – review & editing, Supervision.
Beibei Xu: Writing-Review & Editing, Formal analysis, Supervision, Funding acquisition.

Declaration of Competing Interest

The authors declare that they have no known competing financial interests or personal relationships that could have appeared to influence the work reported in this paper.

Enhancing the economic efficiency of cross-regional renewable energy trading via optimizing pumped hydro storage capacity

Xingjin Zhang[a,b], Edoardo Patelli[c], Ye Zhou[d], Diyi Chen[a,b], Jijian Lian[e], Beibei Xu*[a,b]

[a] *Institute of Water Resources and Hydropower Research, Northwest A&F University, Shaanxi Yangling 712100, China*

[b] *Key Laboratory of Agricultural Soil and Water Engineering in Arid and Semiarid Areas, Ministry of Education, Northwest A & F University, Shaanxi Yangling 712100, China*

[c] *Department of Civil and Environmental Engineering, University of Strathclyde, Glasgow, United Kingdom*

[d] *Institute of Hydraulic Machinery, Department of Operation Support, China Institute of Water Resources and Hydropower Research, Beijing, China*

[e] *Key Laboratory of Hydraulic Engineering Simulation and Safety, Tianjin University, Tianjin 300072, China*

***Corresponding author:** Beibei Xu

Mailing Address: Institute of Water Resources and Hydropower Research, Northwest A&F University, Shaanxi Yangling 712100, China

Telephones: 086-187-0080-9631

E-mail: xubeibei0413@163.com

Abstract

The integration and cross-regional delivery of fluctuating renewable energies are crucial for supporting the decarbonization of energy systems. Although the cross-regional delivery of renewable energy has been widely explored in existing literature, the economic implications of the power delivery modes on the capacity configuration of pumped hydro storage stations (PHSs) remain unexplored. Hence, this paper proposes a game-theoretic based cross-regional energy trading model to analyze how PHS can enhance the economic efficiency of the integrated energy systems. We apply this framework to three typical power delivery models, utilizing a practical cross-regional energy trading case in China, with a focus on the sending-end. Results reveal that a power delivery model that emphasizes minimizing residual load fluctuations significantly curtails deviation power in cross-regional energy trade settlements, constraining it to a mere 5%. Although the augmentation of PHS capacity leads to an increase in the leveling costs of the integrated delivery system, it simultaneously fosters cross-regional integration of renewable energy and bolsters the economic feasibility of long-distance power transmission. These results underscore the effectiveness of the framework introduced and provide valuable insights to inform decisions about power delivery modes and energy storage capacity in future energy and power system planning.

Keywords

Cross-regional renewable energy trading; Pumped hydro storage; Power delivery models; Capacity configuration; Economic efficiency.

1. Introduction

Aligned with the Paris Agreement and ambitious mid-century decarbonization goals, renewable energy (RE) generation is poised for significant expansion, catalyzing the global energy transition [1]. The global installed capacity of RE is expected to exceed 440 GW in 2023, reflecting a year-on-year increase of 107 GW [2]. Given the uneven distribution of RE resources and demand centers, cross-regional transmission of large-scale RE is increasingly seen as a promising solution for the transition to low-carbon power systems [3, 4]. However, as the penetration rate of intermittent RE sources increases, the variability and instability in output may jeopardize the secure and stable operation of the existing power systems [5]. This could lead to a substantial impact on electricity supply costs and pricing, rendering RE unable to meet the requirements for efficient transmission [6]. The incorporation of pumped hydro storage stations (PHSs), with its ability to promptly react to shifts in renewable energy and demand [7], is recognized as a vital measure to improving the grid's secure adaptability for long-distance RE transmission.

PHSs stand as the most mature and cost-efficient energy storage technology [8], ideally suited for large-scale deployment to support the reliable integration of RE [9]. The global capacity of PHS is anticipated to reach 240 GW by 2030, largely propelled by China's intentions to implement an additional 65 PHS projects [10]. However, despite the extensive practical application of PHS, its costs remain relatively significant due to the complex geographical conditions [11] and long construction period [12]. This will inevitably have an impact on the overall economic efficiency of the integrated hydro-wind-solar-storage delivery system (IHDS) at the sending-end. Simultaneously, the adoption of suitable operational strategies can enhance PHS flexibility, improving the smoothness of power delivery [13, 14]. This, in turn, strengthens the competitiveness of the power generated by IHDS in the receiving-end power market. Therefore, a crucial task involves proposing a suitable power delivery model and determining the corresponding PHS capacity for IHDS to enhance the efficiency of cross-regional energy trading.

Three main strategies have been proposed: The first strategy primarily focuses on optimizing system operations and capacity via price-driven demand response (DR) programs. As per the literature review in [15], the peak-valley pricing program reduces the overall electricity demand during peak hours, resulting in an approximately 10% shift in peak load. Shen et al. constructed a multi-objective optimization model for multi-energy storage capacity planning based on coupled price-driven DR, revealing how DR influences energy storage capacity [16]. Kiptoo et al. introduced an integrated optimal planning framework, which effectively reduces mismatches between generation and load profiles by integrating energy storage and dynamic pricing DR [17]. Pan et al. formulated a two-stage optimization model for planning allocation and operational scheduling, utilizing peak-valley price incentives, which improves the economic efficiency of the integrated energy system by 14.8% [18]. Although the implementation of price-driven DR programs proves effective in reducing operational costs, it significantly compromises the power transmission stability of interconnection lines [19].

The second approach examines the complementarity of hybrid energy systems to develop power delivery and planning models. For example, Canales et al. employed a complementarity index as a parameter in an optimization model to define the optimal energy capacity and establish the best operational schedule [20]. Solomon et al. examined how the temporal complementarity of solar and wind resources benefits the power system's reliability and influences storage requirements [21]. Guo et al. introduced a novel generation scheduling approach that considers power transmission stability requirements, with the aim of enhancing complementarity of hybrid energy system [22]. He et al. used the Pearson’s coefficient to analyze complementary features and created a capacity optimization model for hybrid energy systems, reducing curtailment and improving transmission lines utilization [23]. However, these studies failed to coordinate the optimization of both the power supply and the grid load, limiting the realization of synergistic benefits from the interplay between regional generation structures and load characteristics.

The third approach investigates planning and operational issues of power systems, with a focus on minimizing load demand fluctuations. Liu et al. considered local and energy input region demands to develop a day-ahead peak-shaving model for renewable energy, aiming to minimize residual load fluctuations [24]. Zhang et al. analyzed transmission reliability and economic feasibility constraints of IHDS, deducing three screening principles for capacity configuration [25]. Jurasz et al. compared different load demand time series and found that substituting typical daily load profiles for actual demand curves typically leads to underestimating energy costs, up to 15% [26]. Feng et al. tackled the issue of insufficient capacity for flexible sources in regional grids by devising a mixed-integer linear programming model based on minimizing the peak-valley difference of the residual load series that excels at reducing peak power demand compared to alternative models [27].

However, the existing studies primarily focus on evaluating the economic and technical feasibility of capacity configuration while assuming static electricity prices or quantities, neglecting the dynamic nature of energy supply and demand across regions. This compromises the precision of the findings and underplays the value of cross-regional transmission for the IHDS power [28], thus restricting its competitiveness in receiving-end markets. Although cross-regional integration of RE sources enhances power supply reliability, reduces flexibility capacity requirements, and mitigates carbon emissions in receiving-end systems [29-31], from an economic point of view power imports requisition the available power generation space of receiving units, leading to a reduction in their electricity generation benefits [32]. Therefore, it is essential to consider technical and economic aspects of cross-regional RE trading and understanding how economic efficiency interconnect with power delivery modes and PHS capacity configuration of IHDS.

In response to these problems and challenges, this study proposes a cross-regional energy trading framework that integrates the power delivery models of the IHDS with game-theoretic pricing models. Compared with the existing study, the main innovations and contributions of this paper are as follows.

- Three typical power delivery models of IHDS are proposed and evaluated, which respectively focus on the peak-valley electricity price incentive (Model 1), the complementarity of IHDS (Model 2), and the minimization of residual load fluctuations (Model 3).
- A game-theoretic based cross-regional energy trading model is established to assess the potential of PHS in enhancing the economic efficiency of the IHDS.
- A practical engineering case is applied to analyze the calculation results of three different power delivery models and compare their economic adaptability.
- The influence of various delivery modes on the PHS capacity configuration of IHDS is revealed, considering three facets: energy efficiency, cost performance, and transaction feasibility.

The remainder of this paper is organized as follows. Cross-regional power delivery models and trading framework of IHDS are presented in Section 2. Section 3 illustrates the game-theoretic based pricing model and the solution method. The case studies and simulation results are discussed in Section 4. Finally, Section 5 presents the conclusion.

2. Cross-regional power delivery models and trading framework

2.1. System description

The structure of the cross-regional consumption of RE, encompassing both the sending-end and receiving-end power systems is shown in Fig. 1. The sending-end system is comprised of four subsystems: hydropower, wind power, solar power and PHS. Hydropower and PHS play a crucial role in mitigating the fluctuations of wind and solar power, while also providing essential services like peak shaving and reserve to enhance system stability. The receiving-end system is primarily concentrated in areas with high loads and includes hub substations and nearby power plants. Assuming that the generation units of these power plants have a low capacity to meet the load, which mainly comes from thermal power, gas power, nuclear power, etc. These facilities are interconnected through an extensive network to receive external power inputs. The power generated by IHDS is transmitted from the sending-end to the receiving-end via a long-distance and high-capacity Ultra-high-voltage direct current (UHV DC) transmission lines. It is assumed that the receiving-end cannot export electricity back to the sending-end to avoid congestion and limit violations in bidirectional power flow.

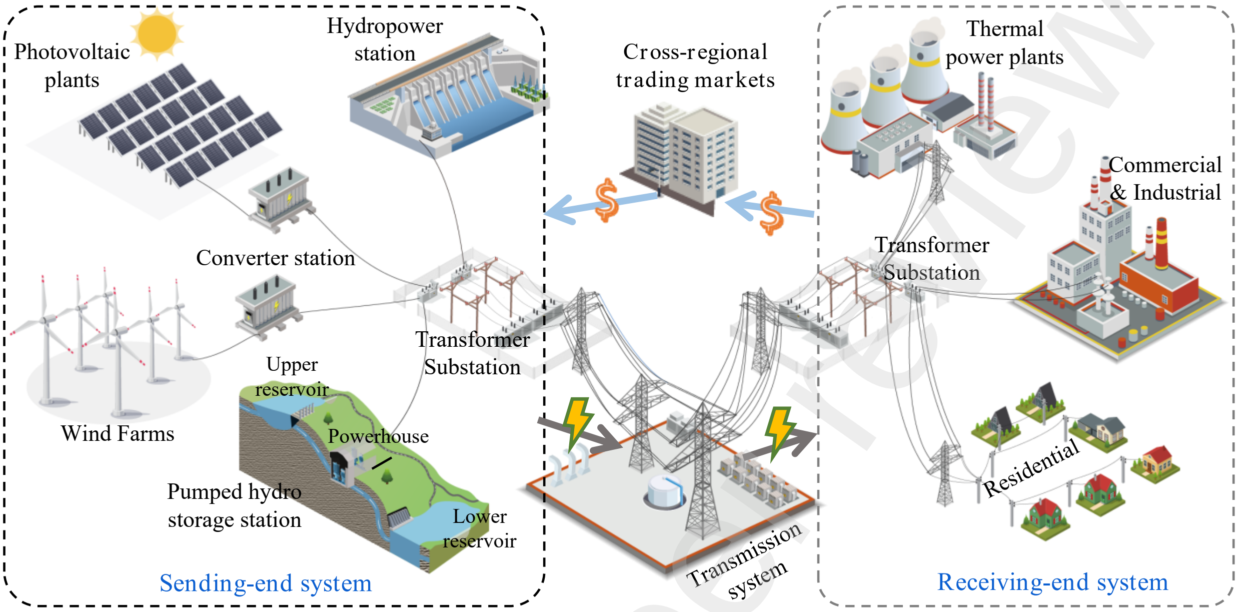

Fig. 1. Structure diagram of the cross-regional consumption of renewable energy.

To enhance the energy efficiency and operational economy of the entire cross-regional trading system, the internal operation of IHDS is optimized at the sending-end region. This optimization process leads to the determination of the most efficient power delivery mode, which is subsequently employed as the transmission curve for IHDS and transmitted to the receiving-end region. At the receiving-end, economic dispatch is achieved by modifying the start-stop status and output of the local unit, considering the transmitted power from the sending-end and local load demands.

2.2. Cross-regional power delivery models

2.2.1. Objectives

The objectives of IHDS for cross-regional transmission can be summarized into two main aspects. Firstly, optimizing the allocation of hydropower and PHS resources to maximize power output efficiency and improve the economic of transmission lines. Secondly, meeting peak load demands of the receiving-end to reduce start-stop cycles of thermal power units and ensure a secure, energy-efficient, and cost-effective operation. Hence, this section presents three typical power delivery models tailored to various optimization objectives of IHDS.

Model 1: By incorporating peak-valley electricity price incentives at the receiving-end, the power delivery plans of IHDS is optimized with the goal of maximizing transmission benefits (R_1).

$$\max R_1 = \sum_{t=1}^{T} \kappa_{opt} P_{Tran,t} - \sum_{t=1}^{T} \left(c_{cur} P_{cur,t} - c_{loss} P_{loss,t} \right) \tag{1}$$

$$\kappa_{opt} = \begin{cases} \kappa_{peak}, t \in T_P \\ \kappa_{flat}, t \in T_F \\ \kappa_{valley}, t \in T_V \end{cases} \tag{2}$$

where t is the simulated time step; T is the simulation period; $P_{Tran,t}$ is power transmission at time t; c_{cur} and c_{loss} are the energy curtailment and load shedding penalty costs, respectively; $P_{cur,t}$ and $P_{loss,t}$ are the energy curtailment and lost load value at time t, respectively; κ_{opt} is the optimal transaction price; κ_{peak}, κ_{flat}, and κ_{valley} are the electricity prices of peak, flat, and valley periods, respectively; T_P, T_F, and T_V represent the peak, flat, and valley periods of load demand, respectively.

This constitutes an optimization operating mode driven by price-based demand response. Its advantage lies in harnessing peak and valley time price signals from the receiving-end grid to proactively guide the sending-end system's units in peak shaving, thus diminishing the load peak and off-peak difference [33]. However, it hampers the coordinated operation capability of cross-regional power resources in integrating RE consumption.

Model 2: This delivery mode is founded on the complementary characteristics of IHDS. The objective is to maximize the power transmission benefit (R_2), as expressed in Eq. (3).

$$\max R_2 = \kappa_{opt} \sum_{t=1}^{T} P_{Tran,t} - \sum_{t=1}^{T} \left(c_{cur} P_{cur,t} - c_{loss} P_{loss,t} \right) \tag{3}$$

This model efficiently harnesses the flexibility adjustment potential of IHDS, facilitating the cross-regional integration of RE. Nonetheless, it overlooks the load demand variation, which could limit its practical applicability, such as potential power shortages due to inadequate regulating capacity in the receiving-end.

Model 3: This delivery mode includes two optimization objectives: one aims to maximize the transmission benefit (R_2) of IHDS, while the other aims to ensuring steady power output from the generating units at the receiving-end, thereby reducing power generation costs. Therefore, the optimization objective in Eq.(4) is defined as minimizing the standard deviation σ_T of the residual load, with the goal of achieving stability in the operation of the receiving-end units.

$$\max \sigma_T = \sqrt{\frac{1}{T} \sum_{t=1}^{T} \left(P_{load,t} - \frac{1}{T} \cdot \sum_{t=1}^{T} \left(P_{load,t} - P_{Tran,t} \right) \right)^2} \tag{4}$$

where $P_{load,t}$ the load demand of the receiving-end at time t.

The advantage of this mode lies in effectively leveraging source-load complementarity between the two regional power grids. It not only enhances the economic efficiency of the sending-end but also smooths the residual load demand curve, thereby reducing peak demand in the receiving-end [34]. However, the multi-objective, nonlinear programming nature of this delivery model escalates the complexity and time required for solution.

2.2.2. Constraints

All three delivery modes described above necessitate adherence to the constraints of each generating subsystem in IHDS (as reported in Appendix, see A.1-A.3), the operational restrictions of the interconnection lines, and power balance constraints, specified as follows:

(1) Stability constraint of power delivery. To prevent frequent adjustments of the DC converters and

ensure the reliability of power transmission, it is advisable to present the transmission power on the DC interconnection lines in a stepwise manner [35].

$$P_{Tran,t} \in \left\{ P_{Tran1}, P_{Tran2}, \cdots, P_{Tran\mathrm{n}} \right\} \tag{5}$$

where $P_{Tran\mathrm{n}}$ are the transmission power during the n^{th} stable operational period within the power transmission curve of IHDS.

(2) Constraint on the time interval for power delivery adjustment. UHV DC power transmission should refrain from repetitive adjustments within a designated time frame. After a single adjustment, to uphold the stability of power transmission, the power must remain constant for a prescribed minimum interval [36].

$$DC_t + DC_{t+\tau-1} \le 1, \forall \tau \in [1, 2, \cdots, K-1] \tag{6}$$

where DC_t is the binary variable, with values of 0 or 1, indicating whether there is an adjustment in DC interconnection line power at time t; K is the minimum time interval for interconnection line power adjustments.

(3) Transmission power variation constraint. To guarantee the stability and reliability of IHDS, it is imperative to impose constraints on the fluctuations in DC interconnection line power export.

$$\left| P_{Tran,t} - P_{Tran,t-1} \right| \le \Delta P_{Tran} \tag{7}$$

where ΔP_{Tran} is the extent of power transmission fluctuations, and its magnitude signifies the transmission line's resilience to power variations.

(4) Transmission capacity constraints. The DC interconnection lines face constraints from both maximum and minimum transmission capacity.

$$P_{Tran,\min} \le P_{Tran,t} \le P_{Tran,\max} \tag{8}$$

where $P_{Tran,min}$ and $P_{Tran,max}$ are the upper and lower capacity limits of UHV DC transmission lines.

(5) Transmission power balance constraint.

$$\sum_{i=1}^{N} P_{i,t}^{HPs} + P_{WTs,t} + P_{PVs,t} + \sum_{m=1}^{M} \left(P_{PHS,t}^{gen,m} - P_{PHS,t}^{pump,m} \right) + P_{loss,t} = P_{Tran,t} \tag{9}$$

$$P_{loss,t} \ge 0 \tag{10}$$

2.3. Renewable energy cross-regional trading framework

In cross-regional energy trading, the sending and receiving ends represent distinct stakeholders, necessitating the consideration of economic benefits for both parties. The benefits for both parties are primarily determined by the cross-regional transaction price and electricity. The sending-end provides power and devises pricing strategies, taking the lead by making proactive decisions. Conversely, the receiving-end formulates decisions that maximize its interests based on the strategies devised by the sending-end, assuming a follower role. Thus, this paper characterizes the interaction between the sending and receiving ends as a non-cooperative Stackelberg game. Fig. 2 depicts a framework of the cross-regional RE trading, integrating the IHDS power delivery modes and a Stackelberg game involving sending and receiving end systems.

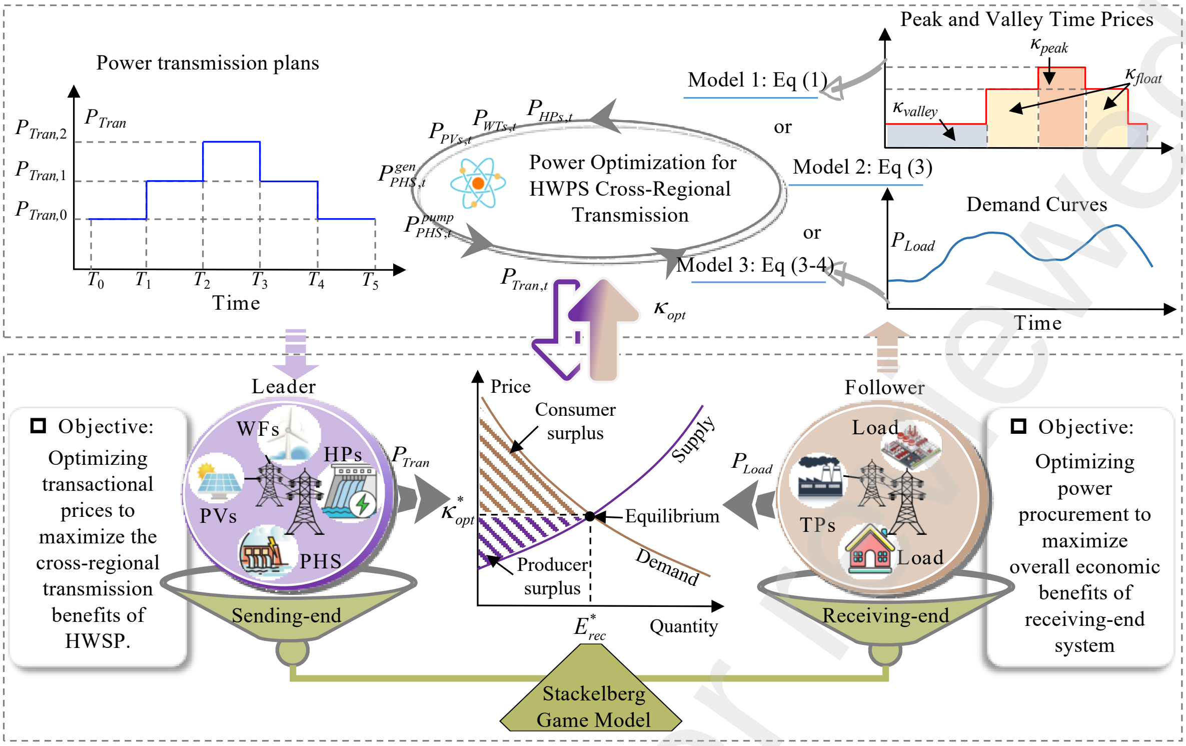

Fig. 2. Framework of cross-regional renewable energy transactions.

In the game interaction, the pricing strategy devised by the sending-end plays a critical role in determining the purchasing electricity at the receiving-end. This price is calculated by considering the IHDS's marginal cost and the transmission cost incurred though transmission lines. It stands as a pivotal factor in motivating the receiving-end to engage in electricity procurement. Significantly, the receiving-end grid can reject electricity from the sending-end in favor of local thermal power generation, albeit at the expense of coal consumption and carbon emissions penalties. If the purchasing price from the sending-end surpasses the cost of coal-based generation, the receiving-end may refrain from procurement or opt for a partial supply. In turn, this constrains the pricing strategy of the sending-end. It must provide an attractive pricing strategy to the receiving-end while ensuring a return on investment [37]. Therefore, the core of cross-regional RE trading rests upon the strategic choices made by these two stakeholders, culminating in the equilibrium achieved within the market's competitive dynamics.

3. Modeling of cross-regional renewable energy trading

This section employs the concepts of Stackelberg game and Nash equilibrium theory to propose a bi-level optimization model for the electricity pricing of IHDS in cross-regional transactions. The main assumptions of the proposed bi-level optimization model are as follows:

(1) The output curves of wind and solar energy are obtained by forecasting, whereas the forecasting errors are disregarded.

(2) The load demand of receiving-end system is assumed to be inelastic to the price signal.

(3) The provider of RE generation at the sending-end region operates in resource-rich areas without performance risks.

(4) All power generation companies in the receiving-end grid are treated as conventional thermal power producers, and the carbon emission coefficients of thermal units remain constant.

3.1. Cross-regional energy trading model

3.1.1. Sending-end system decision model

The sending-end system seeks to maximize the value of dispatched electricity across regions, as expressed in Eq. (11). The profit (M_{sys}) signifies the income derived from selling IHDS power (R_{sys}) after deducting generation expenses, which encompass investment costs (C_{INV}), operation and maintenance costs ($C_{O\&M}$), and remanent value of equipment (C_{SAL}).

$$\max M_{sys} = R_{sys} - C_{INV} - C_{OM} + C_{SAL} \tag{11}$$

$$\begin{cases} R_{sys} = \sum_{t \in T} \kappa_{opt} E_{sys,t} \\ C_{INV} = \sum_{s \in \Omega_{sys}} c_{inv,s} C_s \\ C_{O\&M} = \sum_{s \in \Omega_{sys}} \mu_s c_{inv,s} C_s \\ C_{SAL} = \sum_{s \in \Omega_{sys}} \delta_s c_{inv,s} C_s \end{cases} \tag{12}$$

where E_{sys} is actual electricity sales of IHDS; Ω_{sys} = {*WTs*, *PVs*, *HPs*, *PHS*} is the set of power generation technologies; $c_{inv,s}$ is the unit capacity investment cost ; C_s is the installed capacity; μ_s is operation and maintenance cost factor; δ_s the residual value coefficient.

The constraints of the sending-end system model are as follows:

(1) Cross-regional trading power constraint.

$$0 \le E_{sys,t} \le P_{Tran,t} \Delta t \tag{13}$$

(2) Marginal pricing constraint.

$$\kappa_{opt} \ge \kappa_{\min} + \kappa_{tran} \tag{14}$$

where κ_{min} is the marginal cost price of IHDS; κ_{tran} is the inter-regional transmission price. It is noteworthy that under the peak-valley electricity price guidance method of Model 1, the formula for calculating the transaction price is as follows:

$$\kappa_{opt} = \frac{\kappa_{peak} E_{peak} + \kappa_{flat} E_{flat} + \kappa_{valley} E_{valley}}{E_{peak} + E_{flat} + E_{valley}} \tag{15}$$

where E_{peak}, E_{flat} and E_{valley} are the power generation of IHDS during peak, flat and valley periods, respectively.

(3) Competitive pricing constraint. To enhance the competitiveness of IHDS's power in the receiving-end spot market, it is essential to ensure that the price does not exceed the benchmark electricity price (κ_{BG}) of the receiving-end. This can be expressed as follows:

$$\kappa_{opt} \le \kappa_{BG} \tag{16}$$

3.1.2. Receiving-end system decision model

The receiving-end system determines the optimal electricity procurement to achieve economic dispatch based on the power delivery plan and transaction price provided by the sending-end, as shown in Eq. (17). The profit (M_{rec}) of the receiving-end depends on market transaction revenues and generation costs. Notably, revenues (R_{rec}) are primarily sourced from cross-regional electricity purchases and spot market sales of power generated by local thermal units. Generation costs encompass procurement cost (C_{buy}), coal-fired cost (C_{buy}), and CO_2 emissions cost (C_{CO2}).

$$\max M_{rec} = R_{rec} - C_{buy} - C_{fuel} - C_{CO2} \tag{17}$$

$$\begin{cases} R_{rec} = \kappa_{BG} \sum_{t \in T} \sum_{j \in N_G} P_{j,t}^{G} + \kappa_{BG} \sum_{t \in T} E_{rec,t} \\ C_{buy} = \sum_{t \in T} \kappa_{opt,t} E_{rec,t} \\ C_{fuel} = \sum_{t \in T} \sum_{j \in N_G} \left[a\left(P_{j,t}^{G}\right)^2 + bP_{j,t}^{G} + c \right] \\ C_{CO2} = \pi_{CO2} \sum_{t \in T} \sum_{j \in N_G} \lambda_j P_{j,t}^{G} \end{cases} \tag{18}$$

where $P_{j,t}^{G}$ is the output power of the j^{th} unit, $E_{rec,t}$ is the cross-regional electricity procurement during period t; λ_j is the carbon emissions baseline of the j^{th} unit; π_{CO2} is the emission penalty cost.

In practice, the receiving-end region typically includes a multitude of generating units. Treating each unit's output as a decision variable would lead to an overwhelming number of model variables. Theretofore, the thermal power units in the receiving-end are clustered according to capacity and type, while disregarding transmission capacity limitations in the aggregated grid [38]. The operational constraints of the clustered thermal power units are given in A.4. Besides, the decision model of sending-end incorporates the following constraints.

(1) Electricity procurement constraint.

$$0 \le E_{rec,t} \le P_{load,t} \Delta t \tag{19}$$

(2) Cross-regional interconnection lines power balance. Assuming that the purchasing party typically bears the energy losses of interregional transmission lines, the relationship between the traded electricity of the sending and receiving ends can be described as:

$$E_{rec,t} = \left(1 - l_{tran}\right) E_{sys,t} \tag{20}$$

where l_{Tran} is the loss coefficient of interregional transmission lines.

(3) Load balancing constraint.

$$\sum_{j \in N_G} P_{j,t}^{G} + E_{rec,t} = P_{Load,t} \tag{21}$$

3.1.3. Stackelberg game model

During the process of game interaction, the sending-end assumes the leadership role. It is responsible for optimizing the power delivery plan and setting an ideal cross-regional energy trading price to maximize its profits through encouraging electricity purchases by the receiving-end. Meanwhile, the receiving-side system, acting as a follower, primarily aims to meet load demands while ensuring the economic efficiency. It calculates the optimal electricity procurement to maximize profits, relying on the transaction price provided by IHDS.

For the sending-end, the trading strategy is denoted as κ_{opt}, the return function as M_{sys}, and the trading target is to maximize M_{sys}. The optimal strategy adheres to the following principle:

$$\begin{cases} \kappa_{opt}^{*} = \arg\max_{\kappa_{opt}} M_{sys}\left(\kappa_{opt}, E_{rec,t}^{*}\right) \\ S.t. \quad \text{Eqs.}\,(13-16) \end{cases} \tag{22}$$

where $\kappa^*_{w,t}$ and $E^*_{rec,t}$ are the optimal negotiated price and transaction electricity at the sending and receiving ends when the game's equilibrium, respectively.

For the receiving-end, the trading strategy is denoted as $E_{rec,t}$, the return function as M_{rec}, and the trading target is to maximize M_{rec}. The optimal strategy is guided by the following principle:

$$\begin{cases} E^*_{rec,t} = \arg\max_{E_{rec,t}} M_{rec}\left(\kappa^*_{opt}, E_{rec,t}\right) \\ S.t. \quad \text{Eqs.}\,(19-21)\,\&\,\text{A.4} \end{cases} \tag{23}$$

The optimization problems represented by Eq. (22) and (23) represent the standard equilibrium expression in a Stackelberg game. The IHDS modifies strategy κ_{opt} to maximize M_{sys}, while the receiving-end adapts strategy $E_{rec,t}$ to maximize M_{rec}. If a set of strategies $\{\kappa^*_{w,t}, E^*_{rec,t}\}$ exists, it enable both parties $\{M_{sys}, M_{rec}\}$ to simultaneously achieve maximum values without further improvement through individual strategy adjustments. In this scenario, the electricity price signal serves as the Nash equilibrium price.

3.2. Model solution

The dynamic pricing model based on Stackelberg game proposed in this paper is a high-dimensional, nonlinear characterized by a bi-level structure. Generally, the master-slave game model converts the follower model into constraints using Karush-Kuhn-Tucke (KKT) conditions, forming a mathematical programming problem with equilibrium constraints [39]. Despite its computational speed, the KKT method encounters difficulties when dealing with large-scale nonlinear problems and security concerns related to information [40]. Therefore, a distributed iterative algorithm is utilized to convert the master-slave game problem into sub-problems for the sending and receiving sides, facilitating iterative resolutions. Both sides adapt their strategies reciprocally, engaging in continuous iterations until reaching a Nash equilibrium state or the maximum iteration limit. The solution process for the cross-regional electricity trading model of IHDS is illustrated in Fig. 3. The specific steps are as follows:

Step 1: Data input. This involves providing key information and relevant parameters to the proposed, including meteorological data, equipment specifications, and transmission lines parameters, etc.;

Step 2: RE generation scenario reduction and marginal price calculation. The K-means algorithm proposed in Ref. [41] is applied to reduce wind and solar output scenarios. The marginal electricity price of HIDS is calculated using marginal costs and reasonable utilization hours for different technologies, as shown in Eq. (24).

$$\kappa_{\min} = \frac{\sum_{s\in\Omega_{sys}} \kappa_s C_s \varpi_s + C_{PHS}\gamma_{PHS}}{\sum_{s\in\Omega_{sys}} C_s \varpi_s} \tag{24}$$

where ϖ_s is the reasonable utilization hours; κ_s is the marginal cost; γ_{PHS} is the PHS capacity tariff;

Step 3: Initializing game model equilibrium solution: set $iter = 0$, maximum number of iterations J, and initialize the price of sending-end $\{\kappa^{(0)}_{opt}\}$, the electricity purchase of receiving-end $\{E^{(0)}_{rec,t}\}$, and the convergence error ε;

Step 4: Start iterative solver: $iter \leftarrow iter + 1$;

Step 5: Solving transmission plan: calculate the transmission power $\{P^{(iter)}_{Tran,t}\}$ using the current values of $\{\kappa^{(iter)}_{opt}\}$ combined with the power delivery models. This step is solved using Gurobi solver implemented in Python.

Step 6: Compute receiving-end revenue using the model from Section 3.2.2 incorporating delivery power and transaction price $\{\kappa_{opt}^{(iter)}\}$, and provides feedback on optimized purchase quantity $\{E_{rec,t}^{(iter)}\}$ to the sending-end system.

Step 7: Assessing the game equilibrium achievement. If $iter = J$ or

$$\left|\left\{\kappa_{opt,t}^{(iter)}, E_{rec,t}^{(iter)}\right\} - \left\{\kappa_{opt,t}^{(iter-1)}, E_{rec,t}^{(iter-1)}\right\}\right| \le \varepsilon \tag{25}$$

the Stackelberg game equilibrium solution is identified set $\kappa^* w,t = \{\kappa_{opt}^{(iter)}\}$ and $E^* rec,t.= \{E_{rec,t}^{(iter)}\}$ and continue to Step 8 otherwise return to Step 4.

Step 8: Output results. Providing the optimal transaction prices $\kappa^* w,t$ and transaction quantities $E^* rec,t$.

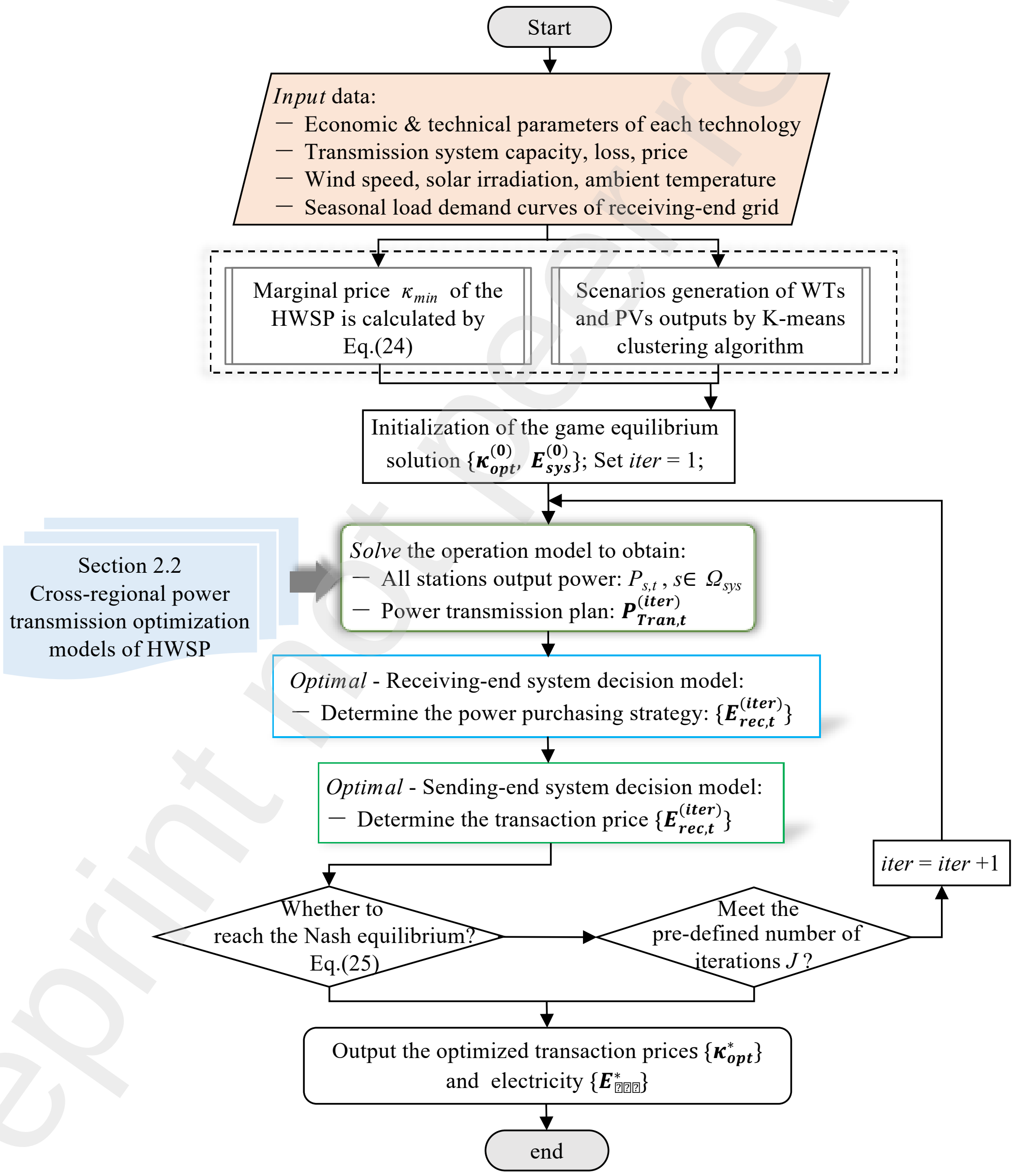

Fig 3. Solution flow chart for the cross-regional renewable energy trading model.

3.3. Evaluation indicators

In this section, evaluation indicators are introduced to assess power delivery modes and capacity configuration of IHDS, emphasizing energy efficiency, cost performance, and transaction feasibility.

3.3.1. Energy efficiency

Storage capacity factor (*SCF*) is introduced as a measure of the potential utilization of PHS by IHDS. It is defined as the ratio of the actual generation supplied by PHS to fill energy deficits over a specific time period [42], which, in this study, spans one year, to the total theoretical generation available. *SCF* can be expressed as:

$$SCF = \frac{\sum_{t \in T} P_{PHS,t}^{gen}}{C_{PHS} \cdot T} \times 100\% \tag{26}$$

where C_{PHS} is the installed capacity of PHS.

A ratio between the actual energy utilized and the nominal RE available, is used to measure Renewable energy utilization (*REU*) [43]. It serves to analyze the comprehensive efficiency of energy utilization and assesses the impact of PHS capacity configuration in enhancing energy usage. REU can be expressed as:

$$REU = \frac{E_{WFs} + E_{PVs} + E_{HPs}}{E_{WFs}^{ava} + E_{PVs}^{ava} + E_{HPs}^{ava}} \tag{27}$$

where E_{WFs}, E_{PVs}, and E_{HPs} are the actual energy contributed to the total transmitted energy by WFs, PVs, and HPs, respectively; E_{WFs}, E_{PVs}, and E_{HPs} are the nominal available energy of WFs, PVs, and HPs, respectively.

Transmission line utilization (*TLU*) serves as a pivotal metric to assess the operational efficiency of transmission lines. It quantifies the ratio of energy transported by transmission lines to the theoretical energy transfer limit within a specific time period. *TLU* can be expressed as follows:

$$TLU = \frac{\sum_{t \in T} P_{Tran,t}}{P_{Tran}^{\max} \cdot T} \times 100\% \tag{28}$$

3.3.2. Cost performance

Renewable energy penetration (*REP*) is employed to investigate the consumption of RE by the receiving-end grid. It is calculated as the percentage of RE generation employed to satisfy the load demand of the receiving-end grid divided by the total load demand [44]. *REP* can be expressed as:

$$REP = \frac{E_{RE \to load}}{E_{Load}} \times 100\% \tag{29}$$

where $E_{RE \to load}$ is the total RE amounts contributed to meet load demand by IRES; E_{load} is the total load demand of receiving-end grid.

Levelized cost of energy (LCOE) stands as a widely adopted metric for assessing the cost performance of IHDS. It represents the per megawatt-hour cost (in discounted real RMB) required to construct and operate IHDS over its assumed financial life and operational cycle [45]. *LCOE* can be expressed as:

$$LCOE = \frac{C_{INV} - \sum_{y \in Y} \frac{D_y}{(1+r)^y} R_{tax} + \sum_{y \in Y} \frac{C_{OM,y}}{(1+r)^y} \left(1 - R_{tax}\right) - \frac{C_{SAL}}{(1+r)^y}}{\sum_{y \in Y} \frac{E_{Total,y}}{(1+r)^y}} \tag{30}$$

$$D = A_0(1-r_s)/Y \tag{31}$$

where D_y is the depreciation of fixed assets in year y; $C_{OM,y}$ is the operations and maintenance expenditures in year y; r is the discount rate; Y is the expected lifetime of IRES; R_{tax} is tax rate; C_{SAL} is the the salvage value of fixed assets; $E_{Total,y}$ is the electricity generation of IRES in year y; A_0 is the original value of the fixed asset, r_s is the net salvage rate.

Levelized cost of CO_2 mitigation (*LCCM*) is a metric employed for evaluating the cost associated with the reduction or mitigation of CO_2 emissions throughout the lifespan of a specific project [46]. Lower *LCCM* values indicate more economically efficient mitigation options. *LCCM* is determined by considering the total life cycle cost and the effective reduction of CO_2 emissions during the operational period [47]. *LCMM* can be expressed as:

$$LCCM = \frac{C_{INV} - \sum_{y\in Y}\frac{D_y}{(1+r)^y}R_{tax} + \sum_{y\in Y}\frac{C_{OM,y}}{(1+r)^y}(1-R_{tax}) - \frac{C_{SAL}}{(1+r)^y}}{\sum_{y\in Y}\frac{\delta_{CO2}\cdot E_{RE\to Load,y}}{(1+r)^y}} \tag{32}$$

where δ_{CO2} is the reduction of CO_2 emissions factor. According to estimates by the National Climate Center, approximately 0.997 kg of CO_2 emissions are avoided per kilowatt-hour (kWh) of consumed renewable energy [48].

3.6.3. Transaction feasibility

Transaction deviation electricity (*TDE*) is a crucial metric in cross-regional market trading, assessing transaction accuracy and deviations from contracted energy schedules [49]. It is calculated as a percentage, derived from the absolute variance between actual transaction electricity and planned transmission electricity relative to the total planned transmission electricity. *TDE* can be expressed as:

$$TDE = \frac{\sum_{t=1}^{T}\left|P_{tran,t}\Delta t - E_{sys,t}\right|}{\sum_{t=1}^{T}P_{tran,t}\Delta t}\times 100\% \tag{33}$$

Return On Investment (*ROI*) serves as a critical metric for gauging the financial feasibility of cross-regional transactions. It quantifies the relationship between net profits derived from projects and the total investment expenditure [50]. A positive *ROI* indicates the project's profit potential, with a higher *ROI* indicating increased profitability, and conversely. *TDE* can be expressed as [51]:

$$ROI = \frac{B_{NP}}{C_{Total}}\times 100\% \tag{34}$$

where B_{NP} is the net profit, which refers to the total revenue of the project minus the total investment expenditure C_{Total}. Note: When calculating the *ROI* of the receiving-end, it assumes that the thermal power units are already operational, excluding consideration of lifecycle costs and concentrating solely on operational and CO_2 emission expenses.

4. Case study

Qinghai Province in northwestern China is renowned for its significant water resources and substantial potential for wind and solar energy development. To support RE growth and align with national energy transition goals, Qinghai Province has established several clean energy demonstration bases [52]. In this study, a clean energy base in the Hainan Tibetan Autonomous Prefecture of Qinghai Province was selected to assess the validity and applicability of the proposed framework. The power generation of clean energy base is transmitted to the load center in Henan Province via UHV DC interconnection lines, as shown in Fig. 4.

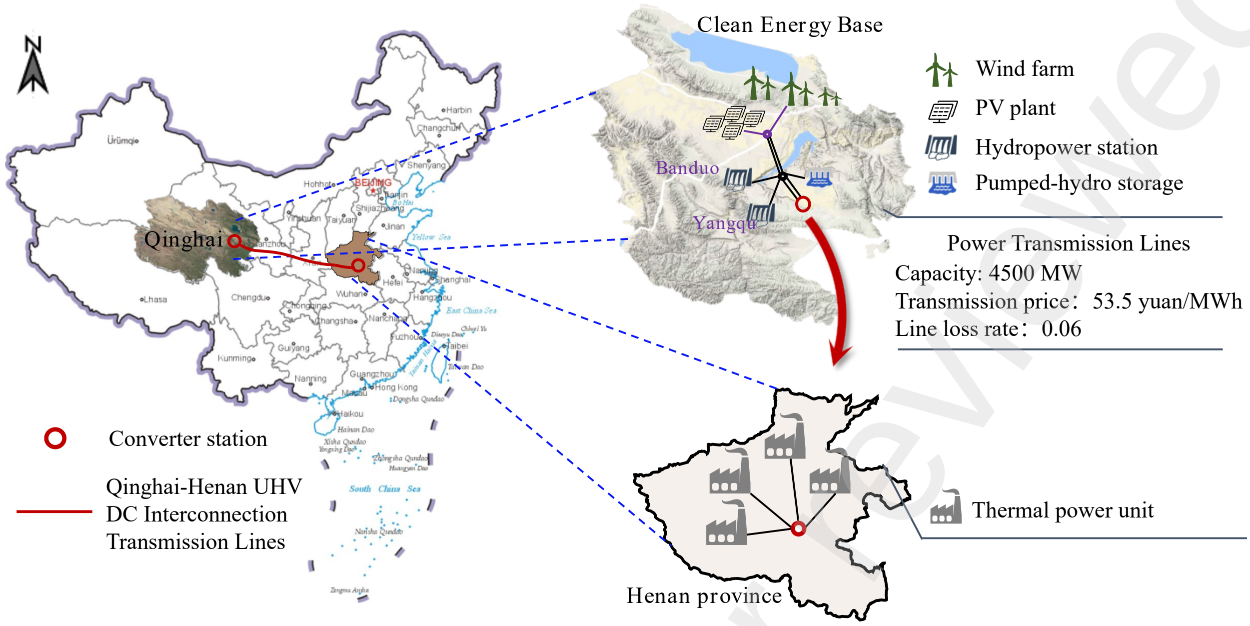

Fig. 4. Schematic diagram of the configuration for the cross-regional energy transmission project.

The sending-end is characterized by the core installation of PHS, comprising the Yangqu and Banduo hydropower stations, along with the surrounding wind and solar power stations. The Bando station has a substantial storage capacity of 15.35 million m^3 and functions as a runoff-type reservoir with a regulating capacity of 1.96 million m^3 [53]. The power station is fitted with three 120 MW units, yielding a cumulative installed capacity of 360 MW. The Yangqu station, located 75 km downstream from the upstream Bando station, operates as a daily regulation power station with a 239 million m^3 regulating capacity. It is presently (i.e. late 2023) under construction, with plans to install three 400 MW units, resulting in a total installed capacity of 1200 MW. The parameters of the two hydropower stations are shown in Table B.1. The planned PHS station, considering geological and altitude factors, has a maximum development capacity of 2000 MW. The parameters for the PHS are determined with reference to Ref. [54] and are presented in Table 1. The planned total installed capacity for wind and solar power station to be integrated to the base is 13 GW. The hourly wind speed, solar irradiance, and temperature data, predicted from historical records, are depicted in Table B.2. The specifications of wind and solar power stations are shown in Table 1.

Table 1. Specifications for wind, solar and pumped-hydro storage power stations

Technology	Parameter	Symbol	Unit	Value
Wind turbine	Rate wind speed	v_r	m/s	13
	Cut-in wind speed	v_{in}	m/s	2.5
	Cut-out wind speed	v_{out}	m/s	32.0
Photovoltaic panel	PV derating factor	f_{PVs}	-	0.80
	Solar irradiance at standard conditions	G_{ref}	W/m^2	1000
	Temperature coefficient	θ_{TC}	-	-0.005
	Temperature at standard conditions	T_{ref}	℃	25
Pumped hydro energy storage	Initial storage capacity	$E_{PHS,0}$	10^7 m^3	2
	Min storage capacity	$E_{PHS,min}$	10^7 m^3	1.06

station	Max storage capacity	$E_{PHS,max}$	10^7 m^3	4.38
	Generation conversion factor	ξ_{gen}	m^3/MWh	780
	Pumping conversion factor	ξ_{pump}	m3/MWh	999
	Maximum start-up times	N_{on}	hour	4

The power transmission line has a maximum capacity of 4500 MW, with a transmission tariff of 0.065 yuan/kWh, and a transmission loss rate of 6%. The model employs a five-segment delivery curve, with each stable transmission period has a minimum duration of 4 hours.

All units in the receiving-end are presumed to be thermal power units, with specific parameters listed in Table B.3. This region adheres to a seasonal time-of-use pricing policy for Peak-valley electricity rates, as established by the Henan Provincial Development and Reform Commission. Specific pricing details are illustrated in Fig. B.1.

To improve computational efficiency, the year is divided into four distinct scenarios (spring, summer, autumn, and winter) marked by significant variations in wind and solar output and load. Subsequently, k-means clustering analysis and scene reduction methods are employed to extract typical output scenarios for each season [55, 56], resulting in three representative scenarios for combined wind and solar power generation. Fig. 5 presents the obtained scenarios for load demand, wind and solar power.

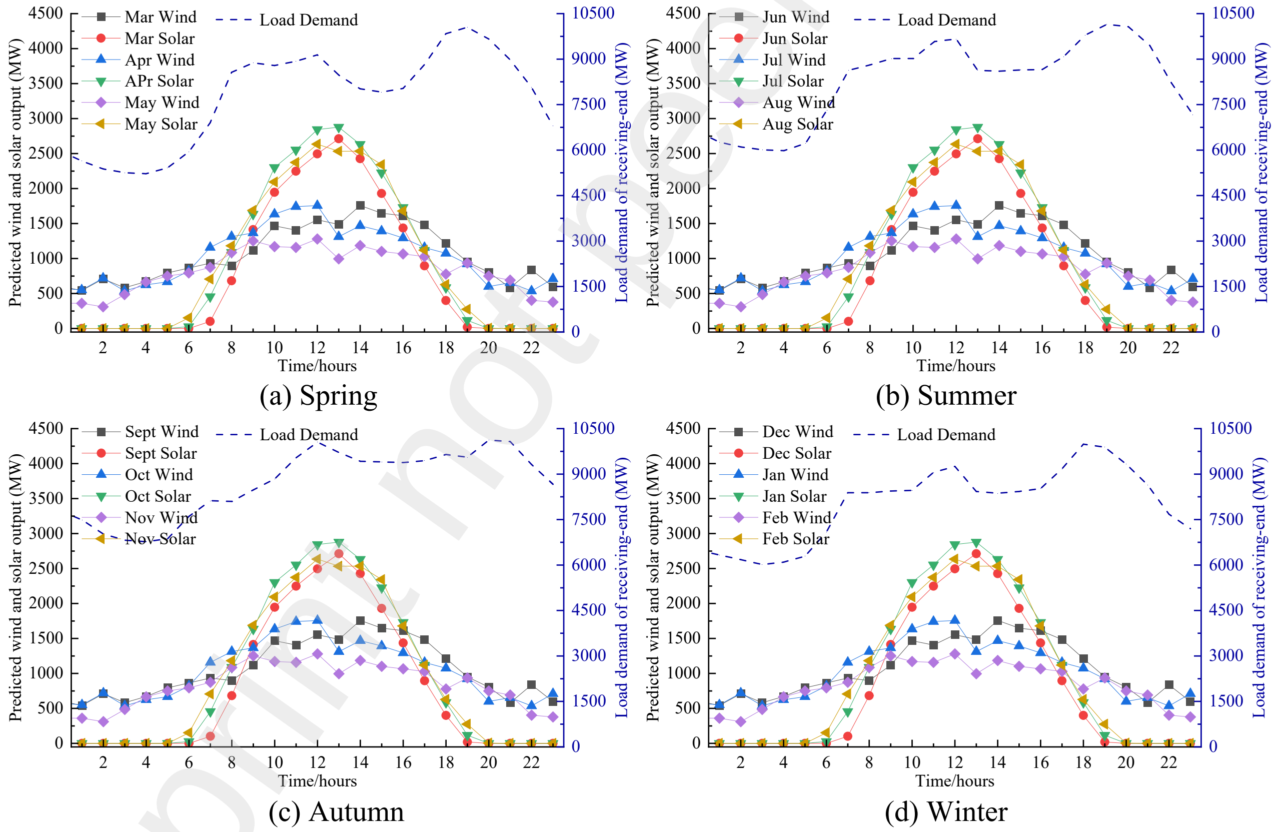

Fig. 5. The typical daily representative wind and solar output scenarios and the typical daily load profiles.

4.1. Energy trading

The accuracy and advantage of three cross-regional delivery models proposed in Section 2.2 are validated through model comparisons. Take the installed capacity of PHS is 1500 MW, coupled with 12500 MW for both wind and solar capacities for instance. Four representative days were randomly selected from each season, and all three models were solved using a consistent optimization framework and algorithm. Fig.6 depicts the power delivery results computed by these three distinct models for representative days in spring, summer, autumn, and winter. Continuous black curves represent the power transmission plans. Transaction price is represented by brown curves. The residual load of the receiving-end system is shown by the black curve with triangles symbols.

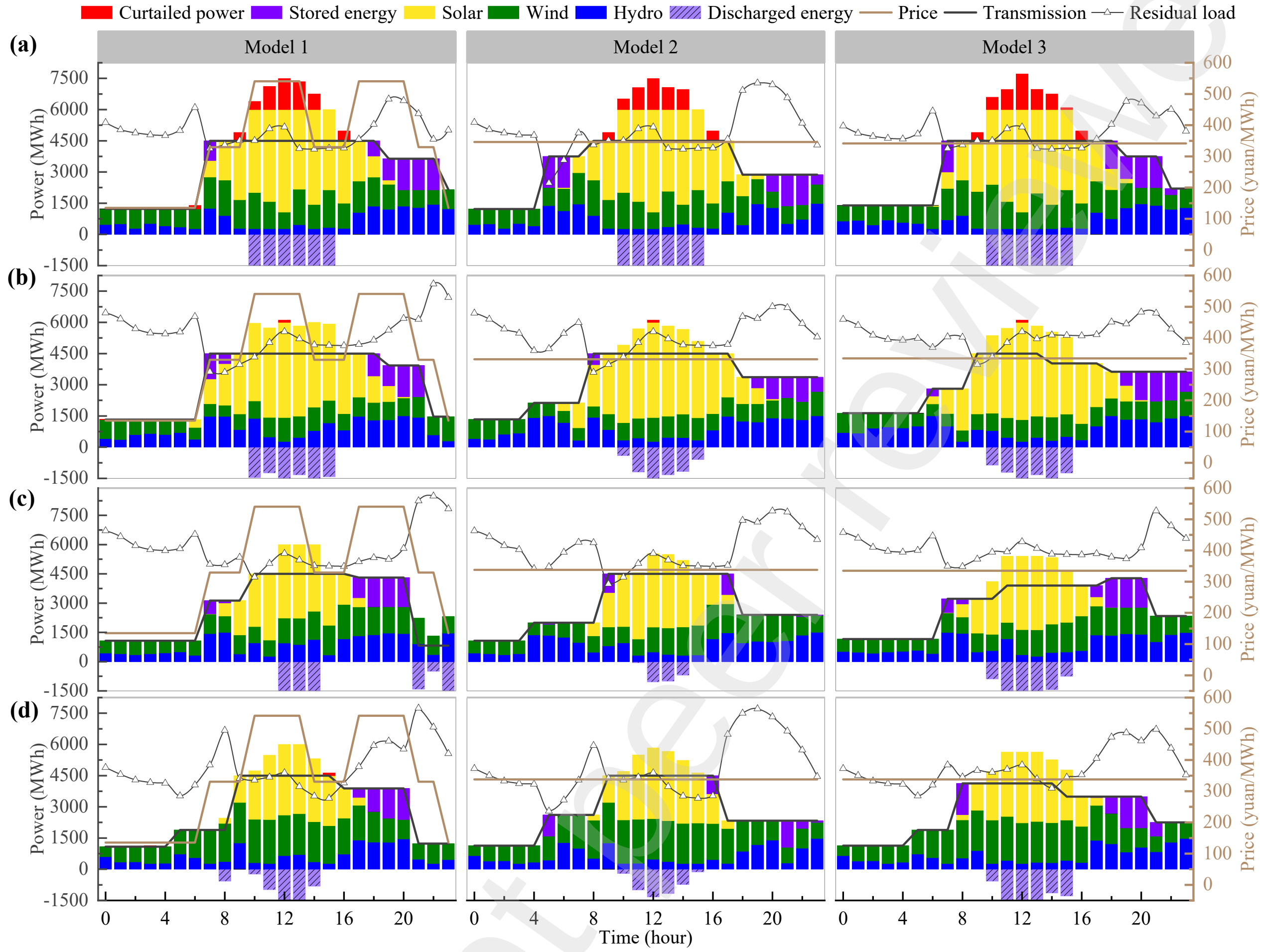

Fig. 6. Seasonal hourly power delivery plans and transaction prices. (a) Spring, (b) summer, (c) autumn, and (d) winter.

By synthesizing the hourly dispatch results of the three models (Fig. 6), the power delivery plans of IHDS exhibit a consistently smooth ladder-like pattern, regardless of the season. This demonstrates that power delivery models introduced in section 2.2 adhere to the requirements for ensuring the smooth operation of RE long-distance transmission. Additionally, the curtailment of IHDS is obviously affected by the seasonal variations. Compared to the output of IHDS in Figs. 6(b-d), the contributions of power generation from wind and solar are greatest in spring, as indicated in Fig. 6(a). Substantial portions (approximately 8.5%) of the potentially available wind and solar resources have to be curtailed in this case due to transmission line and PHS capacity limitations. Integrated over the entire year, overall curtailment is less significant, accounting for only 2% in this case. PHS plays a crucial intermittent role in summer, autumn and winter, but experiences limitations during spring. Energy stored by PHS is deployed primarily during the mid-day hours (10:00- 15:00), coinciding with the peak potential supply from wind and solar power, especially during spring. In all three models, hydropower and wind power play crucial roles as electricity providers during off-peak periods. Collaboratively, they share the responsibility of maintaining the IHDS's essential load operations, thus facilitating seasonal energy complementation.

Comparing the fluctuation of residual load among three delivery models, the smallest fluctuation has been seen in model 3, which is followed by Model 1. This suggests that implementing Model 3's power delivery plans can efficiently diminish the peak-to-valley variation in the receiving-end, demonstrating robust peak-shaving capability, and ensuring the receiving-end grid's efficient and stable operation. Taking the winter scenario (Fig. 6(d)) as an illustration, the peak-to-valley difference rates of residual load, as simulated by Model 1, Model 2, and Model 3, are 56%, 64%, and 48%, respectively.

Furthermore, the duration of peak output for the IHDS also fluctuates according to both the season and delivery model. During spring, when wind and solar resources reach their maximum generation potential, the peak duration of the IHDS's power delivery plan is typically longer. Model 2's operational strategy results in a 12-hour peak duration, whereas Models 1 and 3 surpass this duration by an additional 2 hours. Conversely, during winter when wind and solar resources are scarce, all three delivery models maintain a lower peak duration, approximately 7 hours. Intriguingly, in both autumn and summer, the power delivery plan achieved by Model 3 better matches the peak and off-peak periods of the receiving-end compared to Model 2 and Model 3. For example, in Fig. 6(c), IHDS operates at its lowest output, about 1100 MW, coinciding with the receiving-end system's off-peak period. At 7:00, the IHDS's output rises to around 3100 MW and remains at this level for two-time intervals, which precisely corresponds to the flat period of the receiving-end. At 10:00, IHDS reaches its peak output and maintains about 4500 MW for the subsequent 11 intervals (10:00-20:00), coinciding with the peak period of the receiving-end. This further substantiates the effectiveness of Model 1, emphasizing that the inclusion of time-of-use electricity pricing in the optimization scheduling model enables a close tracking of the peaks and valleys in the receiving-end power system, effectively harnessing the peak-shifting potential of the sending-end grid.

Therefore, models incorporating the load DR of the receiving-end (Model 1 and Model 3) optimize economic and reliable operation, while those excluding it (Model 2) result in increased costs for valley-filling and peak-shaving in the receiving-end.

4.2. Energy efficiency impacts of capacity vs power delivery models

This subsection examines the impact of power delivery models on PHS capacity configuration in the sending-end, with a focus on energy utilization efficiency. Assuming a constant total installed capacity of 13 GW for wind and solar power, three mixed-generation scenarios with varying ratios of wind to solar installation are devised, as indicated in Table 2. For each scenario, the PHS capacity is simulated within the range of [0, 2000] MW, with a simulation increment of 250 MW. Fig. 7 shows the percentage variations in *SCF*, *REU*, and *TLU* influenced by PHS capacity under the operations of Model 1, Model 2, and Model 3 across three distinct scenarios: 40% wind & 60% solar, 50% wind & 50% solar, and 60% wind & 40% solar.

Table 2. Three mixed-generation scenarios with varying ratios of wind to solar installation.

Scenario	Total installed capacity of each technology (MW)			
	Hydropower	Wind power	Solar power	Pumped hydro storage
Scenario 1 (40% wind and 60% solar)	1560	5200	7800	Range [0, 2000], step 250
Scenario 2 (50% wind and 50% solar)	1560	6500	6500	Range [0, 2000], step 250
Scenario 3 (60% wind and 40% solar)	1560	7800	5200	Range [0, 2000], step 250

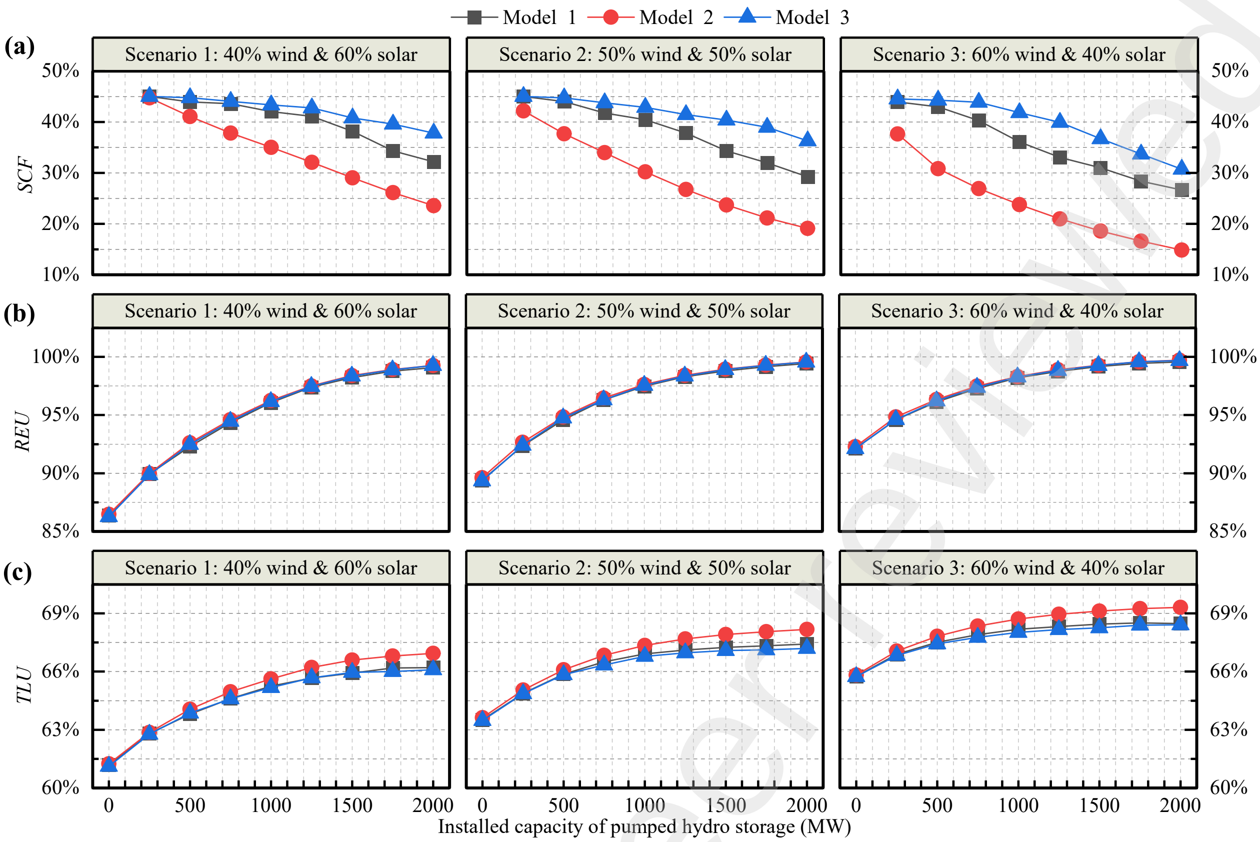

Fig. 7. Percentage variations in energy efficiency indicators resulting from different power delivery models are analyzed across three distinct mixed-generation scenarios. (a) Storage capacity factor (*SCF*), (b) renewable energy utilization (*REU*), and (c) transmission line utilization (*TLU*).

Fig. 7(a) demonstrates a negative correlation between the *SCF* and the installed capacity of PHS. *SCF* exhibits a gradual decline as PHS capacity increases. It should be emphasized that distinct power delivery models lead to substantial differences in the *SCF* decline trend. In the context of Model 2 operation, *SCF* exhibits a linear decrease within the [250, 2000] MW PHS capacity range. Conversely, when implementing Model 1 and Model 2, the decline in *SCF* follows a nonlinear trend. With a consistent wind-solar capacity ratio, the reduction in *SCF* is minimal under Model 3 as PHS capacity increases, followed by Model 1, while Model 2 experiences the most substantial decline. For instance, in Scenario 1, when the PHS capacity is set at 250 MW, all three models yield identical *SCF* values, each at 45%. However, as the storage capacity escalates to 2000 MW, *SCF* decreases to 24% for Model 3, 32% for Model 1, and 38% for Model 2. This signifies that the operational strategy based on Model 1 is more effective in driving PHS facilities to generate economic value.

The *REU*, as depicted in Fig. 7(b), displays a rising tendency as the PHS capacity increases. Remarkably, the upward trajectories for all three models nearly coincide. This indicates that an increased PHS capacity consistently contributes positively to the change in the RE utilization rate, while alterations in the receiving-end load have a negligible impact. Moreover, it's important to observe that achieving equivalent RE generation goals in this case requires smaller pumped storage station capacities when scenarios with a higher wind-to-solar ratio (scenario 3) are selected. For example, to achieve a 97.5% *REU* objective, scenario 1, with a lower wind-to-solar ratio (scenario 1), requires a minimum allocation of 1250 MW in PHS capacity. This amounts to a 20% higher incremental capacity compared to scenario 2 and a 40% greater capacity than scenario 3. This result indicates that in this case, wind and solar resources exhibit a certain degree of complementarity, with wind resources being particularly favorable.

In Fig. 7(b), the *TLU* increases with growing installed capacity of PHS across all energy mix scenarios. This illustrates that increasing the PHS capacity of IHDS makes transmission lines more economically viable. In the same scenario, the *TLU* trends under the three models closely overlap, with differences between any two models not exceeding 1%. The consistent findings across all models suggest that the influence of variations in receiving-end load on the economic efficiency of transmission lines is negligible. Maintaining a constant PHS capacity, scenarios with higher wind energy proportions generally exhibit elevated *TLU* values (C_{PHS} = 500 MW, *TLU* =68%; scenario 3), whereas scenarios with larger solar power proportions tend to yield lower *TLU* values (C_{PHS} = 0 MW, *TLU* =64%; scenario 1). This discrepancy arises from the significantly higher annual effective utilization hours of wind energy compared to solar. Therefore, when optimizing capacity for maximum economic benefit of IHDS, increasing wind power is more effective than solar.

4.3. Cost performance impacts of capacity vs power delivery models

The subsection assesses how varying PHS capacity influences three economic performance indicators: *REP*, *LCOE*, and *LCMM*. Fig. 8 illustrates the variations in *REP*, *LCOE*, and *LCMM* influenced by PHS capacity under three delivery models of IHDS across three distinct scenarios.

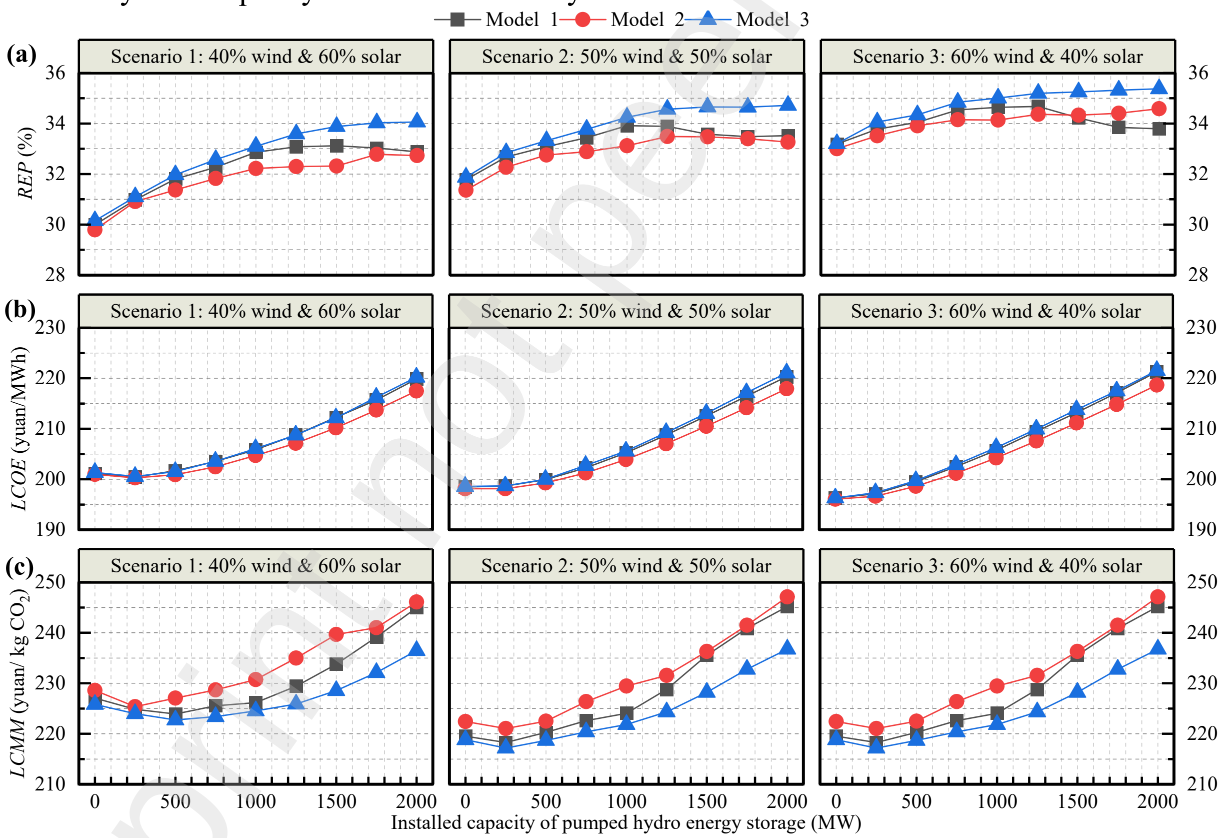

Fig. 8. The effects of changes in capacity and power delivery models on (a) Renewable Energy Penetration (*REP*), (b) Levelized Cost of Electricity (*LCOE*), and (c) Levelized Cost of CO2 Mitigation *(LCCM)* of the integrated hydro-wind-solar-storage delivery system.

For the impact on the *REP* (Fig. 8(a)), PHS capacity configuration of IHDS significantly enhances the share of clean energy electricity at the receiving-end. In various scenarios and across all delivery models, augmenting the PHS capacity by 250 MW in the sending-end can boost *REP* from 30% to 31% compared to scenarios without PHS. As shown in Fig. 8(a), *REP* generally rises and then declines (in Model 1) or gradually levels off (in Models 2 and 3) with increasing PHS capacity. This occurs mainly due to the restricted influence of PHS on the decision-making processes of thermal companies at the receiving-end. Once PHS capacity exceeds a certain threshold, its influence on generation decisions saturates, leading to a stabilized *REP*. Furthermore, with constant PHS capacity, Model 3 operational scheduling consistently achieves higher *REP* in all mixed scenarios.

For the impact on the *LCOE* (Fig. 8(b)), it exhibits a gradual increase with the growth of PHS capacity, and this increase becomes more pronounced with higher capacity levels. In any RE mix scenario, *LCOE* trends under Model 1 and Model 2 closely overlap and are generally higher than those under Model 2. In contrast, the *LCOE* for IHDS exhibits significant variation across various mixed-generation scenarios. Considering the Model 1 as an example, with the PHS capacity ranging from 0 to 2000 MW, the *LCOE* of IHDS in scenarios 1, 2, and 3 increases from 201.1 to 219.8, 198.5 to 220.3, and 196.3 to 211.3 yuan/MWh, correspondingly. This phenomenon indicates that choosing the appropriate delivery model and optimizing capacity ratios of IHDS promotes the cost-effective of the sending-end.

In terms of the impact on *LCCM* (Fig. 8(c)), its value presents a trend of gradual decrease followed by rapid increase as PHS capacity increases. When PHS capacity is below 1000 MW, scenarios with a high wind power proportion significantly reduce *LCCM*. Moreover, across all PHS variations, Model 3 consistently yields lower *LCCM* values than Models 1 and 2. In Scenario 1, Model 3 achieves its lowest *LCCM* of 222.7 yuan/MWh at a 500 MW PHS capacity. At the same capacity, Models 2 and 3 have *LCCM* values of 223.9 and 225.4 yuan/MWh, respectively.

As discussed above, the IHDS employs various delivery models, yielding comparable utilization of effective RE and levelized electricity costs, but differences emerge in power quality and economic performance.

4.4. Transaction feasibility impacts of capacity vs power delivery models

This subsection initially calculates the transaction price between the sending and receiving systems using the game pricing model established in Section 3. Following this calculation, the *TDE* and *ROI* are employed to evaluate the technical and financial feasibility of the cross-regional energy trading project. Fig. 9 presents the variations in power transaction prices and *TDE* values arising from the differences in the power delivery model and installed capacity of IHDS.

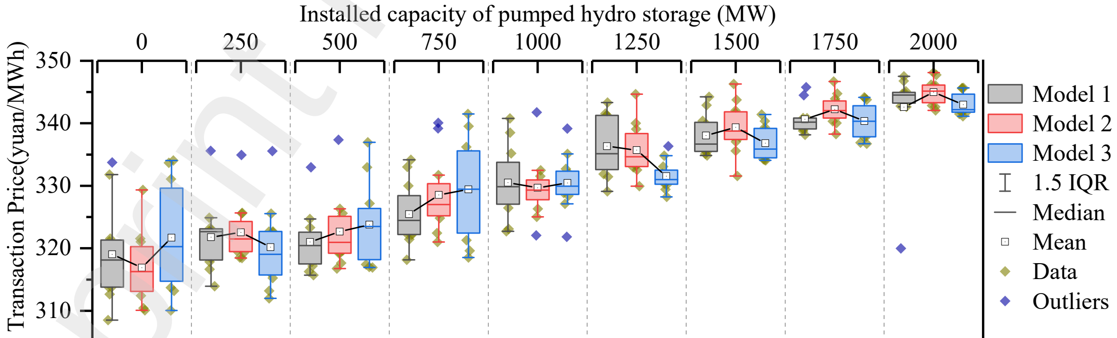

	0	250	500	750	1000	1250	1500	1750	2000	
Model 1	5.81%	5.13%	4.04%	3.84%	2.97%	2.96%	3.23%	3.91%	4.43%	
Model 2	6.60%	5.46%	5.91%	5.86%	5.63%	6.33%	6.87%	5.69%	6.06%	*TDE*
Model 3	5.11%	4.66%	3.59%	2.85%	2.12%	1.40%	0.96%	0.59%	0.63%	

(a) Scenario 1：40% wind and 60% solar.

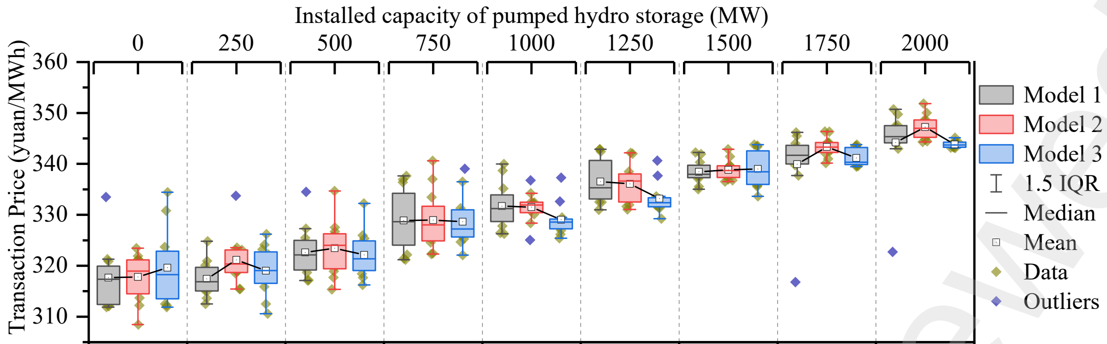

	0	250	500	750	1000	1250	1500	1750	2000	
Model 1	3.65%	2.96%	3.26%	3.14%	2.31%	2.71%	3.86%	4.29%	4.31%	
Model 2	5.21%	4.55%	4.65%	5.41%	5.45%	4.82%	5.22%	5.67%	6.27%	*TDE*
Model 3	3.28%	2.42%	2.48%	1.87%	1.13%	0.47%	0.38%	0.46%	0.38%	

(b) Scenario 2：50% wind and 50% solar.

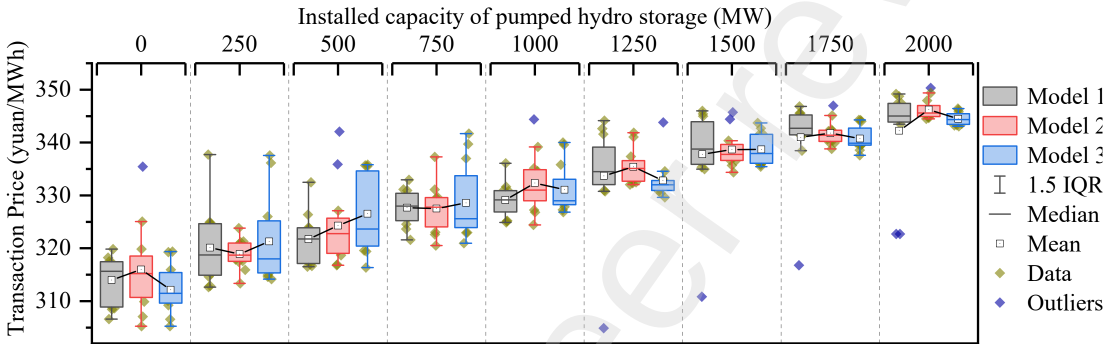

	0	250	500	750	1000	1250	1500	1750	2000	
Model 1	2.75%	2.71%	2.83%	1.96%	2.08%	2.16%	3.73%	4.97%	5.08%	
Model 2	3.44%	3.78%	3.74%	3.79%	4.37%	4.05%	4.42%	4.38%	3.92%	*TDE*
Model 3	2.69%	1.75%	1.81%	0.87%	0.77%	0.44%	0.42%	0.41%	0.28%	

(c) Scenario 3：40% wind and 60% solar.

Fig. 9. The variations in power transaction prices and transaction deviation electricity resulting from the differences in power delivery modes and installed capacity of the integrated hydro-wind-solar-storage delivery system. Boxes represent the 25th and 75th percentiles, and error bars show the 95th percentiles. Black circles and horizontal lines indicate the arithmetic means and medians, respectively. Blue diamonds are outliers.

As depicted in Fig. 9, cross-regional transaction prices generally trend upward as PHS capacity increases for all mixed-generation scenarios and three operational models. The larger the capacity of PHS is, the higher the average transaction price. This implies that configuring a certain capacity of PHS can enhance the transmission quality of IHDS. However, substantial variations exist in inter-regional transaction prices across distinct delivery models. In the absence of configured PHS capacity, annual average transaction prices peak under Model 3 in scenarios 1 and 2, reaching 321.8 and 319.5 yuan/MWh, respectively. Conversely, in scenario 3, Model 2 achieves the highest average transaction price at 315.8 yuan/MWh. This suggests that the choice of IHDS delivery model can have a substantial impact on transaction prices. Additionally, when the PHS capacity reaches 2000 MW, the results from all three scenario sets consistently indicate that Model 1 has the highest transaction price, followed by Model 2, and finally Model 3. This indicates that the impact of PHS capacity on transaction prices varies depending on the delivery model used.

Regarding the *TDE* for cross-regional transactions, it can be observed from Fig. 9 that the *TDE*'s response to increased PHS capacity is non-monotonic, reflecting complex interactions within cross-regional transaction process. At lower PHS capacities, the *TDE* may show volatility due to limited energy storage and RE fluctuations. Increasing PHS capacity improves energy balancing, reducing the

TDE. In 2020, Qinghai Province enacted rules for electricity market trading, allowing a ±5% deviation in electricity quantities, mandating additional evaluation when this threshold is exceeded. Based on this, an examination of *TDE* under different delivery models is conducted. Compared to Models 1 and 2, the IHDS under Model 3 consistently shows significantly lower electricity transaction deviations and maintains a *TDE* within the 5% range, meeting exemption criteria for scrutiny in electricity transactions. This phenomenon reflects the superiority of Model 3 in cross-regional energy trading by ensuring accurate and compliant power transactions within specified deviation ranges for all RE mix scenarios. This is likely due to Model 3's superior efficiency in power scheduling and responsiveness to changes in the receiving-end's load demands.

After identifying the relations in price change, we examine the operational stimulation outcomes of Models 1, 2, and 3 to explore the correlation between increasing PHS capacity and the *ROI* with varying wind-to-solar installation ratios.

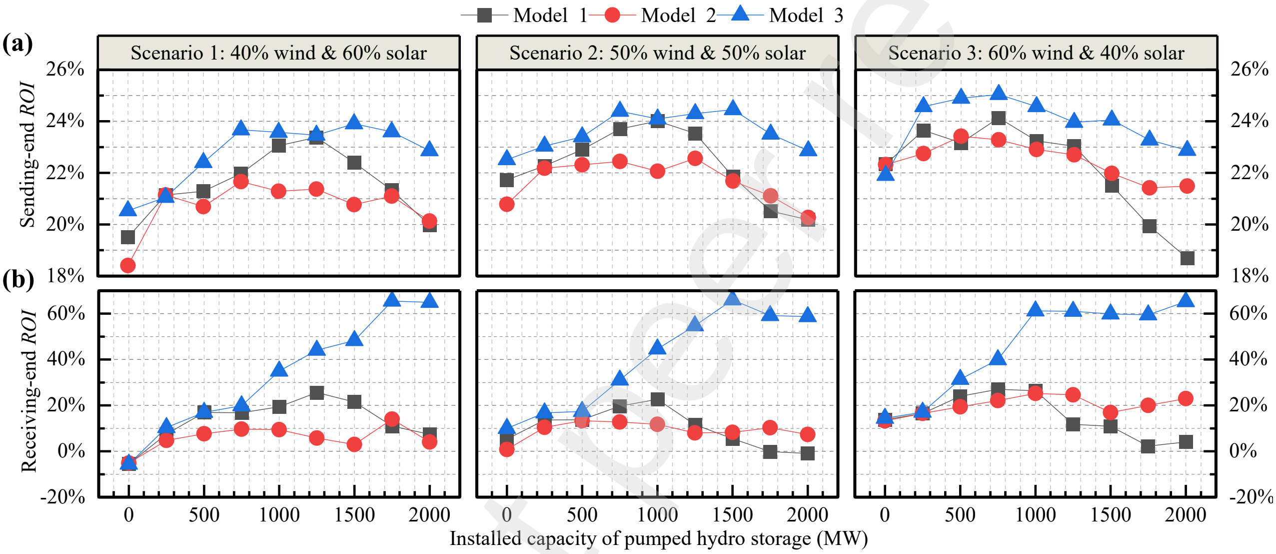

Fig. 10. Impacts of variations in installed capacity and power delivery models of the integrated hydro-wind-solar-storage delivery system on the return on investment (*ROI*) of (a) the sending-end system and (b) the receiving-end system.

Fig. 10 reveals the variation in *ROI* of both the sending-end and receiving-end systems across various scenarios and delivery models in relation to the PHS capacity. In Model 1's operational mode, the *ROI*s of both the sending-end and receiving-end systems initially increase and then decrease. This results in the IHDS's maximum *ROI* corresponding to the PHS capacity that also maximizes the receiving-end system's *ROI*. This indicates that there is an optimal PHS capacity level for maximizing financial returns. However, different wind-to-solar ratios lead to variations in the maximum *ROI*s and their corresponding PHS capacities for both sending and receiving systems. In scenarios 1, 2, and 3, with PHS capacities of 1250 MW, 1000 MW, and 750 MW, the sending-end achieves maximum *ROI*s of 23%, 24%, and 24%, respectively, while the receiving-end reaches 26%, 23%, and 27%. It suggests that the choice of RE mix can significantly impact the economic feasibility of the cross-regional consumption.

Furthermore, in Model 2, both the sending and receiving-end cost-profit rates initially oscillate and then decrease with increasing PHS capacity. With a wind-to-solar ratio of 3:2 and 500 MW of configured PHS capacity, the IHDS reaches a maximum *ROI* of 23%, while the receiving-end corresponds to 19%. In contrast, the *ROI*s for both the sending and receiving-end systems under Model

3 surpassed those of Model 1 and Model 2 as the PHS capacity increased from 0 to 2000 MW. Additionally, in mode 3, the sending-end reached a 25% *ROI* peak at 750 MW of PHS capacity in Scenario 3, with the corresponding receiving-end achieving a 40% *ROI*. This was 13% higher than the *ROI* for the receiving-end system under Model 1 at the same installation level. This suggests that Model 3's delivery strategy is more effective in optimizing *ROI*s and capitalizing on the benefits of increased energy storage.

4.5. Sensitivity analysis of key parameters

In this section, sensitivity analysis was carried to assess the financial feasibility of the proposed cross-regional transaction framework against variation of model input parameters within a range of -10% to +10%, as indicated in Table 3 (left).

Table 3 Sensitivity analysis of various parameters on the financial feasibility.

Parameter	Unit	Value	***ROI*** **of the sending-end system**		***ROI*** **of the the receiving-end system**	
			+10% Base -10%	**Variation**	+10% Base -10%	**Variation**
$c_{inv,PHS}$	yuan/kW	5600		(21.1 ~ 22.6)%		7.6%
$c_{inv,HPs}$	yuan/kW	5775		(21.0 ~ 22.7)%		7.6%
$c_{inv,PVs}$	yuan/kW	3300		(19.7 ~ 24.0)%		7.6%
$c_{inv,WTs}$	yuan/kW	4000		(18.9 ~ 24.8)%		7.6%
π_{CO2}	yuan/t	45		(21.8 ~ 22.1)%		(4.4 ~ 7.6)%
κ_{BG}	yuan/kwh	0.3779		(18.2 ~ 24.8)%		(-7.5 ~ 18.8)%
l_{tran}	%	6		(21.8 ~ 22.3)%		(5.3 ~ 7.6)%
ξ_{pump}	m^3(MWh)$^{-1}$	800		(21.7 ~ 22.9)%		(3.1 ~ 7.6)%
ξ_{gen}	m^3(MWh)$^{-1}$	999		(21.0 ~ 22.8)%		(5.7 ~ 8.4)%
$E_{PHS,0}$	10^7m^3	1.762		(21.8 ~ 22.1)%		(5.4 ~ 7.6)%
C_{PHS}	MW	1500		(20.5 ~ 23.5)%		(2.8 ~ 7.6)%
C_{PVs}	MW	6500		(21.0 ~ 22.2)%		(3.3 ~ 17.4)%
C_{WTs}	MW	6500		(21.5 ~ 21.9)%		(0.4 ~ 14.4)%
			18% 20% 22% 24% 26%		-10% 0% 10% 20%	

The findings of the sensitivity analysis are consolidated in the right columns of Table 3. Among the parameters considered for financial feasibility assessment, the κ_{BG} stands out as the most critical factor. A 10% κ_{BG} increase results in a 3% decrease in the sending-end *ROI* and an 11% reduction in the receiving-end *ROI*. This implies that an increase in κ_{BG} could make the cross-regional energy transaction more economically viable. Besides that, the results show that the *ROI* of the sending-end is sensitive to wind and solar investment costs (in that order), while the *ROI* of the receiving-end is sensitive to solar and wind capacity (in that order). Specifically, when wind and solar investment costs increase by 10%, the *ROI* of the sending-end decreases by about 3% and 2%, respectively, while the *ROI* of the receiving-end remains unaffected. This underscores that the allocation of solar and wind capacity plays a crucial role in determining the financial feasibility of the receiving-end. Research by [57] indicates that wind and solar investment costs have been progressively decreasing over the years. This implies that adopting a phased investment approach when allocating wind and solar capacity can ensure economic feasibility for both the receiving-end and sending-end systems, while preserving technical feasibility. Finally, the *ROI* of both systems shows lower sensitivity to carbon emission costs, line losses, and PHS-related parameters.

5. Conclusions

To unlock the economic efficiency of PHS in cross-regional RE trading, this paper proposes coupling power delivery models with dynamic game-based pricing models. This framework has been applied to a case study involving an integrated hydro-wind-solar-pumped storage system (IHDS) in a Qinghai Province clean energy base. First, a comparative analysis of IHDS power delivery plans among various optimization models confirms that integrating demand response enhances both operational reliability and economic efficiency. During winter, incorporating peak-valley electricity price incentives of and ensuring unit operation stability at the receiving-end within the power delivery model reduces residual load fluctuations by 8% and 16%, respectively, compared to a mode solely maximizing IHDS's complementarity benefit.

The study also explored how IHDS delivery models and PHS capacity impact the economy of cross-regional RE integration. The findings reveal that increasing PHS capacity, despite reducing the storage capacity factor and raising levelized costs for IHDS, stimulates RE integration, enhancing transmission lines economics. Moreover, as PHS capacity increases, the trading price of IHDS rises. Regarding transaction feasibility, a power delivery model that prioritizes minimizing residual load fluctuations significantly limits deviation power in cross-regional energy trade settlements, restricting it to only 5%. Maintaining the installed capacity of IHDS constant, an evaluation of the return on investment (*ROI*) for the sending and receiving systems demonstrates that employing a power delivery mode aimed at minimizing residual load fluctuations yields superior outcomes compared to scenarios solely considering time-based pricing incentives at the receiving end and complementarity performance at the sending end. In a 3:2 wind-to-solar ratio scenario with 750 MW pumped storage capacity, the sending-end achieves a peak 25% *ROI*, while the corresponding *ROI* of receiving-end exceeds Model 1 by 13% with a 40%. Overall, this study underscores the importance of selecting the right operational model and optimizing PHS capacity for IHDS participating in cross-regional transaction to ensure long-term feasibility and sustainability.

The presented work can be further improved to include explicitly market policies, regulations, and environmental considerations. Additionally, this study exclusively addressed electricity trading aspects, yet it's imperative to acknowledge that ancillary services provision significantly impacts the economics of cross-regional energy trading [58, 59]. Therefore, future work should comprehensively explore these factors to tackle challenges from extensive large-scale RE cross-regional consumption.

Funding

This research is supported by National Natural Science Foundation of China (Grant No. K3010121624), Chinese Universities Scientific Fund (Grant No. 2452020210/Z1090220172), Basic and applied basic research fund of Guangdong Province (Grant No. 2021A1515110552), Scientific research fund of Inner Mongolia water resources and Hydropower Survey and Design Institute (Grant No. K4040121228).

CRediT authorship contribution statement

Xingjin Zhang: Conceptualization, Methodology, Software, Formal analysis, Investigation, Data curation, Writing – original draft, Visualization.
Edoardo Patelli: Writing – original draft, Supervision, Writing – review & editing.
Ye Zhou: Methodology, Writing – review & editing, Supervision.
Diyi Chen: Writing - Review & Editing, Funding acquisition, Project administration.
Jijian Lian: Writing – review & editing, Supervision.
Beibei Xu: Writing-Review & Editing, Formal analysis, Supervision, Funding acquisition.

Declaration of Competing Interest

The authors declare that they have no known competing financial interests or personal relationships that could have appeared to influence the work reported in this paper.

Appendix A. Mathematical modeling

A.1. Modeling variable renewable energy

(1) Wind turbine model. The output power of wind turbine (WT) is determined by the wind speed and expressed as a piecewise function.

$$P_{WTs,t} = \begin{cases} 0, & v_t < v_{in}, v_t > v_{out} \\ \dfrac{v_t^3 - v_{in}^3}{v_r^3 - v_{in}^3} \cdot P_{WTs,r}, & v_{in} \le v_t \le v_r \\ P_{WTs,r}, & v_r \le v_t \le v_{out} \end{cases} \tag{A.1}$$

where $P_{WTs,r}$ is the rated power of WT; v_{in} is the cut-in wind speed; v_r is the rated wind speed; v_{out} is the cut out wind speed, v_t is the wind speed at time t.

(2) Photovoltaic panel model. The output power of photovoltaic panel array (PV) is mainly determined by solar radiation intensity, environmental temperature and other factors, as follows:

$$P_{PVs,t} = P_{PVs,r} \cdot f_{PVs} \cdot \frac{G_t}{G_{ref}} \cdot \left[1 + \theta_{Tc}(T_{c,t} - T_{ref})\right] \tag{A.2}$$

where $P_{PVs,r}$ is the PV rated power at reference condition, f_{PVs} is the PV derating factor, G_t is solar radiation at time t, G_{ref} is solar irradiance at standard temperature conduction, θ_{TC} is the PV panel temperature coefficient, $T_{c,t}$ is the operating temperature, T_{ref} is PV array temperature at reference condition.

(3) Capacity constraints of the wind and solar power station is expressed as:

$$\begin{cases} 0 \le P_{WTs,t} \le C_{WTs} \\ 0 \le P_{PVs,t} \le C_{PVs} \end{cases} \tag{A.3}$$

where C_{WTs} and C_{WTs} are the installed capacity of wind farms and solar plants, respectively.

A.2. Hydropower station models

(1) Mass balance

$$\begin{cases} V_{i,t} = V_{i,t-1} + 3600 \cdot \left(Q_{i,t}^{in} - Q_{i,t}^{out}\right)\Delta t \\ Q_{i,t}^{out} = Q_{i,t}^{dis} + Q_{i,t}^{spill} \end{cases} \tag{A.4}$$

where $V_{i,t}$ and $V_{i,t-1}$ are the reservoir storage in time t and t-1,respectively, $Q_{i,t}^{in}$, $Q_{i,t}^{out}$, $Q_{i,t}^{dis}$, and $Q_{i,t}^{spill}$ are the inflow, outflow, penstock release, and water spillage of the i^{th} reservoir, respectively.

(2) Reservoir storage volume limitation

$$V_{\min,i} \le V_{i,t} \le V_{i,\max} \tag{A.5}$$

where V_{min} and V_{max} are the lower and upper limits of the i^{th} reservoir, respectively.

(2) Reservoir characteristics

$$\begin{cases} Z_{i,t}^{up} = f_{ZV,i}\left(V_{i,t}\right) \\ Z_{i,t}^{tail} = f_{ZQ,i}\left(Q_{i,t}^{out}\right) \end{cases} \tag{A.6}$$

where $Z_{i,t}^{up}$ and $Z_{i,t}^{tail}$ are the forebay water level and tailrace water level, respectively, $f_{ZV,i}$ and $f_{ZQ,i}$ are the reservoir storage capacity curve and tailwater rating curve, respectively.

(3) Water level constraints

$$\begin{cases} Z_{\min,i}^{up} \le Z_i^{up} \le Z_{\max,i}^{up} \\ Z_{i,0} = Z_{i,beg} \\ Z_{i,T} = Z_{i,end} \end{cases} \tag{A.7}$$

where $Z_{\min,i}^{up}$ and $Z_{\max,i}^{up}$ are the lower and upper limits of the forebay elevation of the i^{th} reservoir, respectively, $Z_{i,beg}$ and $Z_{i,end}$ are the initial water level at the beginning and the target level at the end of the scheduling period, respectively.

(4) Discharge limitation

$$Q_{\min,i}^{dis} \le Q_{i,t}^{dis} \le Q_{\max,i}^{dis} \tag{A.8}$$

where $Q_{\min,i}^{dis}$ and $Q_{\max,i}^{dis}$ are the lower and upper discharges of the i^{th} reservoir, respectively

(5) Hydro unit output characteristics

$$P_{i,t}^{HPs} = \rho g \eta_{HPs,i} Q_{i,t}^{dis} \Delta H_{i,t} \tag{A.9}$$

$$P_{\min,i}^{HPs} \le P_{i,t}^{HPs} \le P_{\max,i}^{HPs} \tag{A.10}$$

where ρ is the water density, g is the gravitational acceleration, $\eta_{HPs,i}$ is the turbine efficiency, $\Delta H_{HPs,t}$ is the hydraulic head, $P_{\min,i}^{HPs}$ and $P_{\max,i}^{HPs}$ are the maximum and minimum output limits, respectively.

(6) Net hydraulic head

$$\Delta H_{i,t} = \frac{Z_{i,t}^{up} - Z_{i,t-1}^{up}}{2} - Z_{i,t}^{tail} - h_{loss,i} \tag{A.11}$$

where $h_{loss,i}$ is the head loss of the i^{th} hydropower station.

A.3. Pumped hydro storage models

(1) Reservoir capacity constraints

$$\begin{cases} E_{PHS,t} = E_{PHS,t-1} + \xi_{pump} \sum_{m=1}^{M} P_{PHS,t}^{pump,m} - \xi_{gen} \sum_{m=1}^{M} P_{PHS,t}^{gen,m} \\ E_{PHS,\min} \le E_{PHS,t} \le E_{PHS,\max} \end{cases} \tag{A.12}$$

where $E_{PHS,t}$ is the energy storage of the PHS at time t, ξ_{pump} and ξ_{gen} are the pumping and generation conversion factors, respectively, M is is the number of PHS units, $E_{PHS,min}$ and $E_{PHS,max}$ are the minimum and maximum energy storages of the upper reservoir, respectively.

(2) Safe capacity constraint of reservoir

$$\left| E_{PHS,end} - E_{PHS,0} \right| \le E_{PHS,safe} \tag{A.13}$$

where $E_{PHS,safe}$ is the difference in the safe capacity, $E_{PHS,0}$ is the initial storage capacity, $E_{PHS,end}$ is the end storage capacity.

(3) Power generation and pumping constraints

$$u_{PHS,t}^{gen,m} P_{PHS,\min}^{gen,m} \le P_{PHS,t}^{gen,m} \le u_{PHS,t}^{gen,m} P_{PHS,\max}^{gen,m} \tag{A.14}$$

$$u_{PHS,t}^{pump,m} P_{PHS,\min}^{pump,m} \le P_{PHS,t}^{pump,m} \le u_{PHS,t}^{pump,m} P_{PHS,\max}^{pump,m} \tag{A.15}$$

$$0 \le u_{PHS,t}^{gen} + u_{PHS,t}^{pump} \le 1 \tag{A.16}$$

where $u_{PHS,t}^{pump,m}$ and $u_{PHS,t}^{gen,m}$ are the pumping and generation states of the m^{th} PHS unit, respectively, $P_{PHS,\min}^{gen,m}$ and $P_{PHS,\max}^{gen,m}$ are the lower and upper power generation of the m^{th} PHS unit, respectively, $P_{PHS,\min}^{pump,m}$ and $P_{PHS,\max}^{pump,m}$ are the lower and upper power pumping of the m^{th} PHS unit, respectively.

(4) Generation condition constraint. If there is one or more units in power generation condition, the whole PHS station is in power generation state.

$$0 \le u_{PHS,t}^{gen} M - \sum_{m=1}^{M} u_{PHS,t}^{gen,m} \le M \tag{A.17}$$

(5) Pumping condition constraint. If there is one or more units in power pumping condition, the whole PHS station is in power pumping state.

$$0 \le u_{PHS,t}^{pump} M - \sum_{m=1}^{M} u_{PHS,t}^{pump,m} \le M \tag{A.18}$$

(6) PHS unit start-up times

$$\begin{cases} \sum_{t=1}^{T} u_{PHS,t}^{gen,m} \le N_{on}^{gen,m} \\ \sum_{t=1}^{T} u_{PHS,t}^{pump,m} \le N_{on}^{pump,m} \end{cases} \tag{A.19}$$

where $N_{on}^{pump,m}$ and $N_{on}^{gen,m}$ are the maximum power generation and pumping start-up times of the m^{th} PHS unit in scheduling period, respectively.

A.4. Conventional thermal power units

(1) Power output constraints. The output is limited by the available capacity, if the unit is committed:

$$u_{j,t} P_{j,\min}^{G} \le P_{j,t}^{G} \le u_{j,t} P_{j,\max}^{G} \tag{A.20}$$

where $u_{i,t}$ is the status (1/0 mean on/off) of the j^{th} thermal unit at time t, $P_{j,\min}^{G}$ and $P_{j,\max}^{G}$ are the maximum and minimum power output.

(2) Thermal unit ramping constraints:

$$-R_{dn,j}^{G} \le P_{j,t}^{G} - P_{j,t-1}^{G} \le R_{up,j}^{G} \tag{A.21}$$

where $R_{dn,j}^{G}$ and $R_{up,j}^{G}$ is the ramp-down and ramp-up limits of the j^{th} thermal unit, respectively.

(3) Minimum up and down times:

$$\begin{cases} \sum_{\tau=t}^{t+T_{on,j,t-1}} u_{j,\tau} \geq T_{on,j,t}\left(u_{j,t} - u_{j,t-1}\right) \\ \sum_{\tau=t}^{t+T_{off,j,t-1}} u_{j,\tau} \geq T_{off,j,t}\left(u_{j,t-1} - u_{j,t}\right) \end{cases} \tag{A.22}$$

where $T_{on,i,t}$ and $T_{off,i,t}$ is the minimum continuous startup and shutdown time of the j^{th} thermal unit, respectively, and τ is the time index symbol.

Appendix B. Techno-economic database parameters values

Table B.1 Characteristic parameters of hydropower stations.

Technical parameter	Unit	Hydroelectric power station	
		Banduo	Yangqu
Normal storage water level	m	2760	2715
Level of dead water	m	2757	2710
Normal reservoir capacity	10^7 m^3	0.830	147.24
inactive storage	10^7 m^3	0.634	123.34
Installed capacity	MW	360	1200
Guaranteed output of turbine	MW	46.1	228
Maximum discharge	m^3/s	1119.48	1186.2
Average annual energy generation	GWh	1412	4900

Table B.2 Monthly meteorological data at renewable energy base.

Month	Reservoir inflow (m^3/s)	Average wind speed (m/s)	Daily radiation (kWh/m^2/day)	Daily temperature (℃)
January	144	4.16	3.25	-10.88
February	155	4.51	4.16	-6.8
March	345	5.3	5.07	-1.38
April	249	5.16	6.07	3.95
May	648	4.41	6.07	8.39
June	1847	3.89	5.82	11.98
July	924	3.82	5.92	14.18
August	1019	3.66	5.59	13.37
September	859	3.45	4.71	8.83
October	632	3.61	4.24	2.76
November	287	4.07	3.58	-3.92
December	199	4.19	2.98	-9.39

Table B.3 Economic parameters for the integrated hydro-wind-solar-storage delivery system.

Economic parameter	Unit	Hydro	Wind	Solar	PHS
Investment cost	yuan/kW	5775	4000	3300	5600
Life cycle	year	30	20	20	40
Composite depreciation rate	%	3.3	6.3	6.3	2.4
Operation & maintenance cost rate	%	2.3	2.9	1.9	2.7
Marginal electricity price	yuan/kWh	0.230	0.324	0.285	0.354

Capacity Tariff	yuan/kW	-	-	-	617

Table B.4. Technical parameters of thermal power units of the receiving-end system.

Technical parameters	Unit	unit #1	unit #2	unit #3	unite #4
Minimum power output	MW	110	300	600	1000
Maximum power output	MW	20	120	300	500
Ramp up/down limit	MW/h	20	30	60	80
On-off minimum duration	hour	3	3	6	80.0147
Carbon dioxide emissions	kg/MWh	872.9	872.9	817.7	817.7
Coal consumption coefficient a	yuan/MWh^2	0.0175	0.0147	0.0161	0.0035
Coal consumption coefficient b	yuan/MWh	157.78	158.9	173.04	1450.53
Coal consumption coefficient c	yuan	1750	4900	5880	7000
Number of units	-	10	10	7	2
Total installed capacity	MW	1100	3000	4200	2000

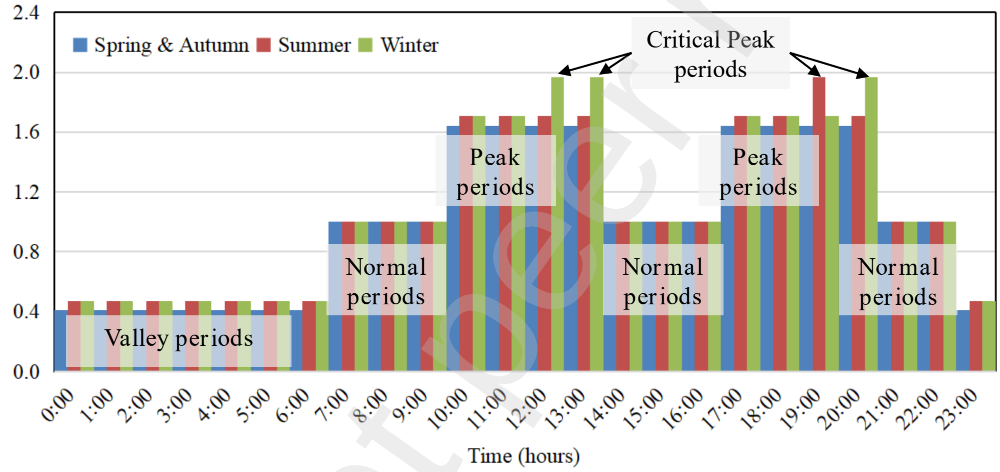

Fig. B.1. Monthly electricity price information of the receiving-end system.

References

[1] Levin T, Bistline J, Sioshansi R, Cole WJ, Kwon J, Burger SP, et al. Energy storage solutions to decarbonize electricity through enhanced capacity expansion modelling. Nature Energy. 2023. https://doi.org/10.1038/s41560-023-01340-6

[2] Agency IE. Renewable Energy Market Update - June 2023. IEA.Paris. https://doi.org/https://www.iea.org/reports/renewable-energy-market-update-june-2023

[3] Zhuo Z, Du E, Zhang N, Nielsen CP, Lu X, Xiao J, et al. Cost increase in the electricity supply to achieve carbon neutrality in China. Nature Communications. 2022;13. https://doi.org/10.1038/s41467-022-30747-0

[4] Aghahosseini A, Bogdanov D, Barbosa LSNS, Breyer C. Analysing the feasibility of powering the Americas with renewable energy and inter-regional grid interconnections by 2030. Renewable and Sustainable Energy Reviews. 2019;105:187-205. https://doi.org/https://doi.org/10.1016/j.rser.2019.01.046

[5] Fan J-L, Li Z, Huang X, Li K, Zhang X, Lu X, et al. A net-zero emissions strategy for China's power sector using carbon-capture utilization and storage. Nature Communications. 2023;14:5972. https://doi.org/10.1038/s41467-023-41548-4

[6] Santos SF, Gough M, Fitiwi DZ, Silva AFP, Shafie-Khah M, Catalão JPS. Influence of Battery

Energy Storage Systems on Transmission Grid Operation With a Significant Share of Variable Renewable Energy Sources. IEEE Systems Journal. 2022;16:1508-19. https://doi.org/10.1109/JSYST.2021.3055118

[7] Mohamed A, Rigo-Mariani R, Debusschere V, Pin L. Stacked revenues for energy storage participating in energy and reserve markets with an optimal frequency regulation modeling. Applied Energy. 2023;350. https://doi.org/10.1016/j.apenergy.2023.121721

[8] Aghahosseini A, Breyer C. Assessment of geological resource potential for compressed air energy storage in global electricity supply. Energy Conversion and Management. 2018;169:161-73. https://doi.org/https://doi.org/10.1016/j.enconman.2018.05.058

[9] Hua Z, Ma C, Lian J, Pang X, Yang W. Optimal capacity allocation of multiple solar trackers and storage capacity for utility-scale photovoltaic plants considering output characteristics and complementary demand. Applied Energy. 2019;238:721-33. https://doi.org/https://doi.org/10.1016/j.apenergy.2019.01.099

[10] Mahfoud RJ, Alkayem NF, Zhang Y, Zheng Y, Sun Y, Alhelou HH. Optimal operation of pumped hydro storage-based energy systems: A compendium of current challenges and future perspectives. Renewable and Sustainable Energy Reviews. 2023;178:113267. https://doi.org/https://doi.org/10.1016/j.rser.2023.113267

[11] Jurasz J, Piasecki A, Hunt J, Zheng W, Ma T, Kies A. Building integrated pumped-storage potential on a city scale: An analysis based on geographic information systems. Energy. 2022;242. https://doi.org/10.1016/j.energy.2021.122966

[12] Barbour E, Wilson IAG, Radcliffe J, Ding Y, Li Y. A review of pumped hydro energy storage development in significant international electricity markets. Renewable and Sustainable Energy Reviews. 2016;61:421-32. https://doi.org/https://doi.org/10.1016/j.rser.2016.04.019

[13] Zhao Z, Ding X, Behrens P, Li J, He M, Gao Y, et al. The importance of flexible hydropower in providing electricity stability during China's coal phase-out. Applied Energy. 2023;336:120684. https://doi.org/https://doi.org/10.1016/j.apenergy.2023.120684

[14] Pattnaik A, Dauda AK, Panda A. Optimal utilization of clean energy and its impact on hybrid power systems incorporating STATCOM and pumped hydro storage. Renewable and Sustainable Energy Reviews. 2023;187:113713. https://doi.org/https://doi.org/10.1016/j.rser.2023.113713

[15] Yan X, Ozturk Y, Hu Z, Song Y. A review on price-driven residential demand response. Renewable and Sustainable Energy Reviews. 2018;96:411-9. https://doi.org/10.1016/j.rser.2018.08.003

[16] Shen Y, Hu W, Liu M, Yang F, Kong X. Energy storage optimization method for microgrid considering multi-energy coupling demand response. Journal of Energy Storage. 2022;45. https://doi.org/10.1016/j.est.2021.103521

[17] Kiptoo MK, Lotfy ME, Adewuyi OB, Conteh A, Howlader AM, Senjyu T. Integrated approach for optimal techno-economic planning for high renewable energy-based isolated microgrid considering cost of energy storage and demand response strategies. Energy Conversion and Management. 2020;215. https://doi.org/10.1016/j.enconman.2020.112917

[18] Pan C, Jin T, Li N, Wang G, Hou X, Gu Y. Multi-objective and two-stage optimization study of integrated energy systems considering P2G and integrated demand responses. Energy. 2023;270. https://doi.org/10.1016/j.energy.2023.126846

[19] Niu J, Tian Z, Zhu J, Yue L. Implementation of a price-driven demand response in a distributed energy system with multi-energy flexibility measures. Energy Conversion and Management.

2020;208. https://doi.org/10.1016/j.enconman.2020.112575
[20] Canales FA, Jurasz J, Beluco A, Kies A. Assessing temporal complementarity between three variable energy sources through correlation and compromise programming. Energy. 2020;192. https://doi.org/10.1016/j.energy.2019.116637
[21] Solomon AA, Kammen DM, Callaway D. Investigating the impact of wind–solar complementarities on energy storage requirement and the corresponding supply reliability criteria. Applied Energy. 2016;168:130-45. https://doi.org/https://doi.org/10.1016/j.apenergy.2016.01.070
[22] Guo Y, Ming B, Huang Q, Wang Y, Zheng X, Zhang W. Risk-averse day-ahead generation scheduling of hydro–wind–photovoltaic complementary systems considering the steady requirement of power delivery. Applied Energy. 2022;309. https://doi.org/10.1016/j.apenergy.2021.118467
[23] He Y, Hong X, Wang C, Qin H. Optimal capacity configuration of the hydro-wind-photovoltaic complementary system considering cascade reservoir connection. Applied Energy. 2023;352. https://doi.org/10.1016/j.apenergy.2023.121927
[24] Liu B, Lund JR, Liao S, Jin X, Liu L, Cheng C. Peak Shaving Model for Coordinated Hydro-Wind-Solar System Serving Local and Multiple Receiving Power Grids via HVDC Transmission Lines. IEEE Access. 2020;8:60689-703. https://doi.org/10.1109/access.2020.2979050
[25] Zhang X, Elia Campana P, Bi X, Egusquiza M, Xu B, Wang C, et al. Capacity configuration of a hydro-wind-solar-storage bundling system with transmission constraints of the receiving-end power grid and its techno-economic evaluation. Energy Conversion and Management. 2022;270:116177. https://doi.org/https://doi.org/10.1016/j.enconman.2022.116177
[26] Jurasz J, Guezgouz M, Campana PE, Kies A. On the impact of load profile data on the optimization results of off-grid energy systems. Renewable and Sustainable Energy Reviews. 2022;159. https://doi.org/10.1016/j.rser.2022.112199
[27] Feng Z-k, Niu W-j, Cheng C-t. Optimal allocation of hydropower and hybrid electricity injected from inter-regional transmission lines among multiple receiving-end power grids in China. Energy. 2018;162:444-52. https://doi.org/10.1016/j.energy.2018.08.045
[28] Crozier C, Baker K. The effect of renewable electricity generation on the value of cross-border interconnection. Applied Energy. 2022;324:119717. https://doi.org/https://doi.org/10.1016/j.apenergy.2022.119717
[29] Guo F, van Ruijven BJ, Zakeri B, Zhang S, Chen X, Liu C, et al. Implications of intercontinental renewable electricity trade for energy systems and emissions. Nature Energy. 2022;7:1144-56. https://doi.org/10.1038/s41560-022-01136-0
[30] Wang W, Li G, Guo J. Large-Scale Renewable Energy Transmission by HVDC: Challenges and Proposals. Engineering. 2022;19:252-67. https://doi.org/10.1016/j.eng.2022.04.017
[31] Jia Z, Wen S, Wang Y. Power coming from the sky: Economic benefits of inter-regional power transmission in China. Energy Economics. 2023;119. https://doi.org/10.1016/j.eneco.2023.106544
[32] Meng Y, Cao Y, Li J, Liu C, Li J, Wang Q, et al. The real cost of deep peak shaving for renewable energy accommodation in coal-fired power plants: Calculation framework and case study in China. Journal of Cleaner Production. 2022;367:132913. https://doi.org/https://doi.org/10.1016/j.jclepro.2022.132913
[33] Yao R, Lu X, Zhou H, Lai J. A Novel Category-Specific Pricing Strategy for Demand Response in Microgrids. IEEE Transactions on Sustainable Energy. 2022;13:182-95. https://doi.org/10.1109/TSTE.2021.3106329
[34] Yuan W, Xin W, Su C, Cheng C, Yan D, Wu Z. Cross-regional integrated transmission of wind

power and pumped-storage hydropower considering the peak shaving demands of multiple power grids. Renewable Energy. 2022;190:1112-26. https://doi.org/https://doi.org/10.1016/j.renene.2021.10.046

[35] Zhong H, Xia Q, Ding M, Zhang H. A new mode of HVDC tie-line operation optimization for maximizing renewable energy accommodation. Dianli Xitong Zidonghua/Automation of Electric Power Systems. 2015;39:36-42. https://doi.org/10.7500/AEPS20140529005

[36] Xu F, Ding Q, Han H, Xie L, Lu M. Power Optimization Model and Analysis of HVDC Tie-line for Promoting Integration of Inter-regional Renewable Energy Accommodation. Automation of Electric Power Systems. 2017;41:152-9. https://doi.org/10.7500/AEPS20170401001

[37] Roberts MB, Sharma A, MacGill I. Efficient, effective and fair allocation of costs and benefits in residential energy communities deploying shared photovoltaics. Applied Energy. 2022;305:117935. https://doi.org/https://doi.org/10.1016/j.apenergy.2021.117935

[38] Pavičević M, Mangipinto A, Nijs W, Lombardi F, Kavvadias K, Jiménez Navarro JP, et al. The potential of sector coupling in future European energy systems: Soft linking between the Dispa-SET and JRC-EU-TIMES models. Applied Energy. 2020;267:115100. https://doi.org/https://doi.org/10.1016/j.apenergy.2020.115100

[39] Zhong J, Li Y, Wu Y, Cao Y, Li Z, Peng Y, et al. Optimal Operation of Energy Hub: An Integrated Model Combined Distributionally Robust Optimization Method With Stackelberg Game. IEEE Transactions on Sustainable Energy. 2023;14:1835-48. https://doi.org/10.1109/TSTE.2023.3252519

[40] Sinha A, Soun T, Deb K. Using Karush-Kuhn-Tucker proximity measure for solving bilevel optimization problems. Swarm and Evolutionary Computation. 2018;44. https://doi.org/10.1016/j.swevo.2018.06.004

[41] Yaghoubi-Nia M-R, Hashemi-Dezaki H, Halvaei A. Optimal stochastic scenario-based allocation of smart grids' renewable and non-renewable distributed generation units and protective devices. Sustainable Energy Technologies and Assessments. 2021;44:101033. https://doi.org/10.1016/j.seta.2021.101033

[42] Javed M, Jurasz J, McPherson M, Dai Y, Ma T. Quantitative evaluation of renewable-energy-based remote microgrids: curtailment, load shifting, and reliability. Renewable and Sustainable Energy Reviews. 2022;164:112516. https://doi.org/10.1016/j.rser.2022.112516

[43] Zhang X, Lian J, Tao Y, Ma C, Chen D, Chen M, et al. Capacity tariff mechanism of a pumped hydro storage station: Pricing approaches for reducing benefit allocation unfairness of integrated renewable energy systems. Journal of Energy Storage. 2023;71:108156. https://doi.org/https://doi.org/10.1016/j.est.2023.108156

[44] Chen Y, Xu J, Wang J, Lund P, Wang D. Configuration optimization and selection of a photovoltaic-gas integrated energy system considering renewable energy penetration in power grid. Energy Conversion and Management. 2022;254:115260. https://doi.org/10.1016/j.enconman.2022.115260

[45] Fattahi A, Sijm J, Van den Broek M, Gordón RM, Dieguez MS, Faaij A. Analyzing the techno-economic role of nuclear power in the Dutch net-zero energy system transition. Advances in Applied Energy. 2022;7:100103. https://doi.org/https://doi.org/10.1016/j.adapen.2022.100103

[46] Wei N, Sheng-nan L, Jiao Z, Xiao-chun L. A possible contribution of carbon capture, geological utilization, and storage in the Chinese crude steel industry for carbon neutrality. Journal of Cleaner Production. 2022;374:133793. https://doi.org/10.1016/j.jclepro.2022.133793

[47] Zong Z, Cai G, Tabbara M, Chester Upham D. CO2-negative fuel production using low-CO2 electricity: Syngas from a combination of methane pyrolysis and dry reforming with techno-economic analysis. Energy Conversion and Management. 2023;277:116624. https://doi.org/https://doi.org/10.1016/j.enconman.2022.116624

[48] Li J, Zhao Z, Xu D, Li P, Liu Y, Mahmud MA, et al. The potential assessment of pump hydro energy storage to reduce renewable curtailment and CO2 emissions in Northwest China. Renewable Energy. 2023;212. https://doi.org/10.1016/j.renene.2023.04.132

[49] Wang W, Zheng S, Fan R, Chen W, Zhou S. Performance Evaluation Index and Method of Micro-Grid Distributed Electricity Trading Under the Background of "Carbon Peaking and Carbon Neutrality". Journal of Shanghai Jiaotong University. 2022;56. https://doi.org/10.16183/j.cnki.jsjtu.2021.391

[50] Bakhshi R, Sandborn PA. A Return on Investment Model for the Implementation of New Technologies on Wind Turbines. IEEE Transactions on Sustainable Energy. 2018;9:284-92. https://doi.org/10.1109/TSTE.2017.2729505

[51] Indra T, Geumpana T, Rizwanul Fattah IM, Mahlia T. Techno-Economic Analysis of Hybrid Diesel Generators and Renewable Energy for a Remote Island in the Indian Ocean Using HOMER Pro. Sustainability. 2022;14:9846. https://doi.org/10.3390/su14169846

[52] Ma C, Gou H. Utilization of Water Conserved by Interprovincial Renewable Energy Substitution for Thermal Power: Incremental Benefits and Advanced Reservoir Operation Rules. Journal of Hydrology. 2023;622:129713. https://doi.org/10.1016/j.jhydrol.2023.129713

[53] Zhang Y, Ma C, Lian J, Pang X, Qiao Y, Chaima E. Optimal photovoltaic capacity of large-scale hydro-photovoltaic complementary systems considering electricity delivery demand and reservoir characteristics. Energy Conversion and Management. 2019;195:597-608. https://doi.org/10.1016/j.enconman.2019.05.036

[54] Gu H, Zhou H, Peng C, Hu Y, Zhao X, Xie J, et al. A Multi-Time Scale Scheduling Model for Power Generation System with High Proportion of New Energy IncludingPumped Storage Power Station. Journal of Shanghai Jiaotong University. 2023:1-22. https://doi.org/10.16183/j.cnki.jsjtu.2023.123

[55] Ma C, Liu L. Optimal capacity configuration of hydro-wind-PV hybrid system and its coordinative operation rules considering the UHV transmission and reservoir operation requirements. Renewable Energy. 2022;198:637-53. https://doi.org/10.1016/j.renene.2022.08.048

[56] Liu Z, He X. Balancing-oriented hydropower operation makes the clean energy transition more affordable and simultaneously boosts water security. Nature Water. 2023;1:778-89. https://doi.org/10.1038/s44221-023-00126-0

[57] Aghahosseini A, Bogdanov D, Breyer C. Towards sustainable development in the MENA region: Analysing the feasibility of a 100% renewable electricity system in 2030. Energy Strategy Reviews. 2020;28:100466. https://doi.org/https://doi.org/10.1016/j.esr.2020.100466

[58] Pérez-Díaz J, Lafoz M, Burke F. Integration of fast acting energy storage systems in existing pumped‐storage power plants to enhance the system's frequency control. Wiley Interdisciplinary Reviews: Energy and Environment. 2019;9. https://doi.org/10.1002/wene.367

[59] Glismann S. Ancillary Services Acquisition Model: Considering market interactions in policy design. Applied Energy. 2021;304:117697. https://doi.org/https://doi.org/10.1016/j.apenergy.2021.117697